Economic Geology, v. XXX, no. XX, pp. X–X

Textural Characteristics of Barren and Mineralized Colloform Quartz Bands at the Low-Sulfidation Epithermal Deposits of the Omu Camp in Hokkaido, Japan: Implications for Processes Resulting in Bonanza-Grade Precious Metal Enrichment

Lauren R. Zeeck,[1] Thomas Monecke,[1,†] T. James Reynolds,[2] Erik R. Tharalson,[1] Katharina Pfaff,[1] Nigel M. Kelly,[1,3] and Quinton T. Hennigh[4]

[1]*Center for Mineral Resources Science, Department of Geology and Geological Engineering, Colorado School of Mines, 1516 Illinois Street, Golden, Colorado 80401, USA*

[2]*FLUID INC., 1401 Wewatta St. #PH3, Denver, Colorado 80202, USA*

[3]*Bruker Nano Analytics, 415 N. Quay Street, Kennewick, Washington 99336, USA*

[4]*Irving Resources, 901 E. 9th Avenue, Longmont, Colorado 80504, USA*

Abstract

The Miocene low-sulfidation epithermal deposits of the Omu camp in northeastern Hokkaido, Japan, are small past-producers of precious metals and represent significant exploration targets for high-grade Au and Ag ores. The quartz textures of ore samples and the distribution of ore minerals within quartz veins were studied to identify the processes that resulted in the bonanza-grade precious metal enrichment in these deposits. In the high-grade vein samples, which are crustiform or brecciated in hand specimen, ore minerals exclusively occur within colloform quartz bands. High-magnification microscopy reveals that ore-bearing colloform bands consist of fine-grained quartz exhibiting relic microsphere textures and quartz having a mosaic texture that formed through recrystallization of the microspheres. The presence of relic microspheres is evidence that the microcrystalline quartz hosting the ore minerals formed through recrystallization of a noncrystalline silica precursor phase. The ore-hosting colloform bands composed of agglomerated microspheres alternate with barren colloform quartz bands that are composed of fibrous chalcedonic quartz and mosaic quartz formed through recrystallization of the chalcedony. The findings of this study are consistent with previous models linking bonanza-grade precious metal enrichment and the formation of bands of noncrystalline silica in low-sulfidation epithermal veins to episodic vigorous boiling or flashing of the hydrothermal system in the near-surface environment.

Introduction

The Omu camp in the Kitami region of northeast Hokkaido, Japan, is host to several small past-producers of precious metals (Watanabe, 1995) and represents the focus of an ongoing exploration program for high-grade, low-sulfidation epithermal Au and Ag ores. Located in the back-arc region of the present Kuril volcanic arc front, the Kitami region is one of Japan's major epithermal provinces. Historic precious metal production in the area yielded a total of ~2.9 Moz Au and ~44.7 Moz Ag (Watanabe, 1995), with minor past production of base metals and mercury (Maeda, 1997).

High-grade ore in the low-sulfidation epithermal deposits of the Omu camp is confined to crustiform banded and brecciated quartz veins. Similar to other low-sulfidation epithermal deposits (Takeuchi and Shikazono, 1984; Matsuhisa and Aoki, 1994; Shimizu et al., 1998; Faure et al., 2002; Leavitt et al., 2004; Sanematsu et al., 2006; Camprubí and Albinson, 2007; Shimizu, 2014), the ore minerals occur within specific colloform quartz bands in the crustiform vein samples. These mineralized colloform quartz bands alternate with barren bands, suggesting that precious metal deposition was episodic. The reasons for the episodic nature of the ore-forming processes are currently not well understood. Previous research at the Sleeper deposit in Nevada and McLaughlin in California demonstrated that electrum in mineralized bands can occur as dendrites that are intergrown with fine-grained colloform quartz formed through recrystallization from a gel-like, noncrystalline silica precursor phase (Saunders, 1990, 1994, 2012; Saunders and Schoenly, 1995; Sherlock and Lehrman, 1995; Saunders et al., 2011). Moncada et al. (2012) and Shimizu (2014) proposed that rapid deposition of the noncrystalline precursor may occur as a result of vigorous boiling or flashing of the thermal waters forming low-sulfidation epithermal deposits, implying that colloform bands containing ore minerals are formed by processes that differ from those resulting in the formation of barren quartz bands.

The present contribution reports on a detailed petrographic study carried out on high-grade vein material from the Omu camp that aimed to establish the textural characteristics of the ore-bearing colloform bands and differences from barren bands. The distribution of ore minerals on the hand specimen scale was determined by micro-X-ray fluorescence (μXRF) analysis. Textures of ore-bearing and barren quartz bands were then systematically studied by high-magnification optical microscopy. The study of the ore mineralogy using reflected-light microscopy, field emission-scanning electron microscopy, and electron microprobe analysis showed that the ore minerals occur only in two texturally distinct types of quartz, with all other quartz types being essentially barren. Ore minerals are present in colloform quartz consisting

†Corresponding author: e-mail, tmonecke@mines.edu

 Submitted: January 16, 2019 / Accepted: July 26, 2020

of relic microspheres originally composed of a noncrystalline silica precursor phase, and in bands of finely crystalline quartz having a mosaic texture interpreted to have formed as a result of recrystallization of a noncrystalline silica precursor phase occurring as microspheres. The textural characteristics of mineralized bands differ from other colloform bands that are primarily composed of chalcedonic quartz. A model is proposed that may explain the link between quartz microtextures and the mechanisms of precious metal deposition.

Geologic Setting

Subduction of the Pacific plate along the eastern margins of the Eurasian and Okhotsk plates was initiated in the Eocene, resulting in the development of the Northeast Japan and Kuril arcs (Jackson et al., 1975). Back-arc extension during the Oligocene to middle Miocene caused the formation of the Japan, Yamato, and Kuril basins (Kimura and Tamaki, 1986). During the early to middle Miocene, the Eurasian and Okhotsk plates collided. This collision is recorded by the deposition of coarse clastic rocks in the Kitami region of northern Hokkaido and a hiatus in volcanic activity along the Kuril arc (Watanabe, 1995).

Back-arc extension in the Kitami region of northern Hokkaido has occurred since the middle to late Miocene. Volcanism, mainly composed of andesite and rhyolite with minor amounts of basalt and dacite, occurred along north-south structural trends in the eastern Omu-Kamikawa and western Monbetsu-Rubeshibe zones (Fig. 1; Watanabe, 1995, 1996). Volcanism commenced at around 14 Ma in the northern part of both zones and gradually migrated to the south with back-arc volcanism occurring until 9 Ma in the Omu-Kamikawa zone and 6 Ma in the Monbetsu-Rubeshibe zone. In the Omu-Kamikawa zone, felsic volcanic rocks overlie basaltic andesites and are in turn overlain by andesite. Rhyolite lavas predominate in the north, whereas welded deposits of dacitic composition are abundant in the south. In the Monbetsu-Rubeshibe zone, felsic lavas and pyroclastic rocks overlie andesitic deposits. At 6 Ma, bimodal volcanism in the back arc ended, with most of the subsequent Pliocene to Quaternary volcanism only occurring near the present arc front (Watanabe 1995, 1996).

Middle to late Miocene hydrothermal activity in the Kitami region was closely associated with felsic volcanism in the back arc of the Kuril arc. Hydrothermal activity resulted in the formation of a large number of low-sulfidation epithermal deposits, most of which are vein-type deposits, although disseminated-type ores are also present. The ore zones are typically located near or within felsic intrusions and lavas, although some of the mercury deposits also occur in sedimentary basement rocks (Watanabe 1995, 1996). The ages of the epithermal deposits closely follow the volcanic activity and shifted over time from north to south. Individual deposits yielded adularia K-Ar ages ranging from 14.3 ± 0.3 to 4.51 ± 0.62 Ma (Watanabe, 1995; Maeda, 1997).

Geology of the Omu Camp

The Omu camp was mapped in 1966 by the Geological Survey of Hokkaido providing the foundation for the present understanding of the local geologic setting of the low-sulfidation epithermal deposits (Fig. 2; Suzuki et al., 1966). Mapping showed that basement rocks locally crop out in the northwestern part of the Omu camp (Suzuki et al., 1966). These rocks belong to the Mesozoic Hidaka Supergroup, which forms part of the N-trending Hidaka-Tokoro metamorphic belt transecting much of central and northern Hokkaido (Okada, 1982; Watanabe and Iwata, 1987). In the study area, the Hidaka Supergroup is primarily composed of slate with thin intercalated sandstone beds.

The oldest Miocene rocks in the Omu camp form part of the 14.3 ± 1.0 Ma (Watanabe, 1995) Kamiômu Formation. This formation crops out extensively in the southern part of the camp where it is composed of sandstone, shale, breccia, tuff, and minor conglomerate that have a north-south strike and dip shallowly (10°–20°) to the east (Suzuki et al., 1966). The Kamiômu Formation is overlain by plagioclase-phyric basaltic andesite of the Nakahoronai lava, which has been dated at 12.9 ± 0.5 Ma (Watanabe et al., 1991). The slightly younger Motoineppu lava yielded an age of 12.0 ± 0.9 Ma (Koshimizu and Kim, 1987). This lava is of dacitic to rhyolitic composition and contains quartz, plagioclase, and biotite phenocrysts (Takanashi et al., 2012). It represents the main host of low-sulfidation epithermal deposits in the Omu camp (Fig. 2; Suzuki et al., 1966). The augite-hypersthene-phyric Inashibetsu lava crops out extensively in the southern part of the camp (Suzuki et al., 1966) and has been dated at 9.8 ± 0.5 Ma (Watanabe and Yamaguchi, 1988). Augite-hypersthene-phyric andesite of the Miocene (Watanabe, 1995) Maru-yama lava is composed of coherent and breccia facies that are mostly exposed in the western and southern parts of the camp.

Sandstone, shale, and tuff of the Pliocene Onishi Formation occur in the southeast. Augite-hypersthene-phyric andesite of the Kamiômu lava represents the youngest Pliocene deposits in the area. Pleistocene augite-hypersthene-phyric andesite of the Numa-dake lava occurs only in the northwestern part of the Omu camp (Fig. 2). Pleistocene and Holocene cover rocks include terrace and floodplain deposits (Suzuki et al., 1966).

The Hokuryu deposit (Fig. 2) was the most significant mine in the Omu camp. Discovered in 1918, the mine produced ~350,000 metric tons (t) of ore at a grade of 8 g/t Au and 33 g/t Ag between 1928 and 1943. High-grade ores were recovered from a NE-striking vein zone over a strike length of 240 m and downdip for over 210 m at grades ranging from 7 to 29 g/t Au. In addition, an E-striking vein zone was exploited that extended 320 m along strike and 160 m downdip at grades of 10 to 30 g/t Au. Additional drilling was conducted between 1965 and 1974, but the mine was not reopened (Barrett et al., 2018).

The Omui deposit in the eastern part of the camp was discovered in 1919 following earlier placer gold recovery in the area. Mining took place from 1920 to 1921 and 1925 to 1928, with minor production in 1933. In total, 22,300 t of ore were extracted at Omui for a total of ~11,000 oz Au and ~270,000 oz Ag. The major E-W–striking quartz vein at Omui, the so-called Honpi vein, was exploited over a strike length of 120 m from four working levels to a depth of 90 m. The 1.0- to 1.5-m-wide vein averaged 21.5 g/t Au and 600 g/t Ag. Adjacent narrow (30–60 cm) veins assayed 3 to 7 g/t Au and 7 to 56 g/t Ag. Drilling in 1984 to 1985 intersected narrow banded veins of variable grade (<1–26.8 g/t Au and 1–1,139 g/t Ag). The old workings are today collapsed to surface (Barrett et

al., 2018). Recent drilling encountered significant vein mineralization. This included vein intercepts grading 96.5 g/t Au and 65.7 g/t Ag over 0.30 m, 46.3 g/t Au and 22.1 g/t Ag over 0.80 m, 38.5 g/t Au and 128 g/t Ag over 0.62 m, and 29.6 g/t Au and 36.5 g/t Ag over 1.10 m (Irving Resources, press releases January 17, 2020, and February 7, 2020).

Additional minor production in the Omu camp is reported to have occurred at the Omu mine (Fig. 2). Initial mining activity occurred in the second half of the 1920s. Between 1938 and 1943, two NE-striking veins were exploited grading 4.3 to 6.5 g/t Au and 28 to 33 g/t Ag. One vein had a strike of 40° and dipped at 70° to the southeast, with a strike length of

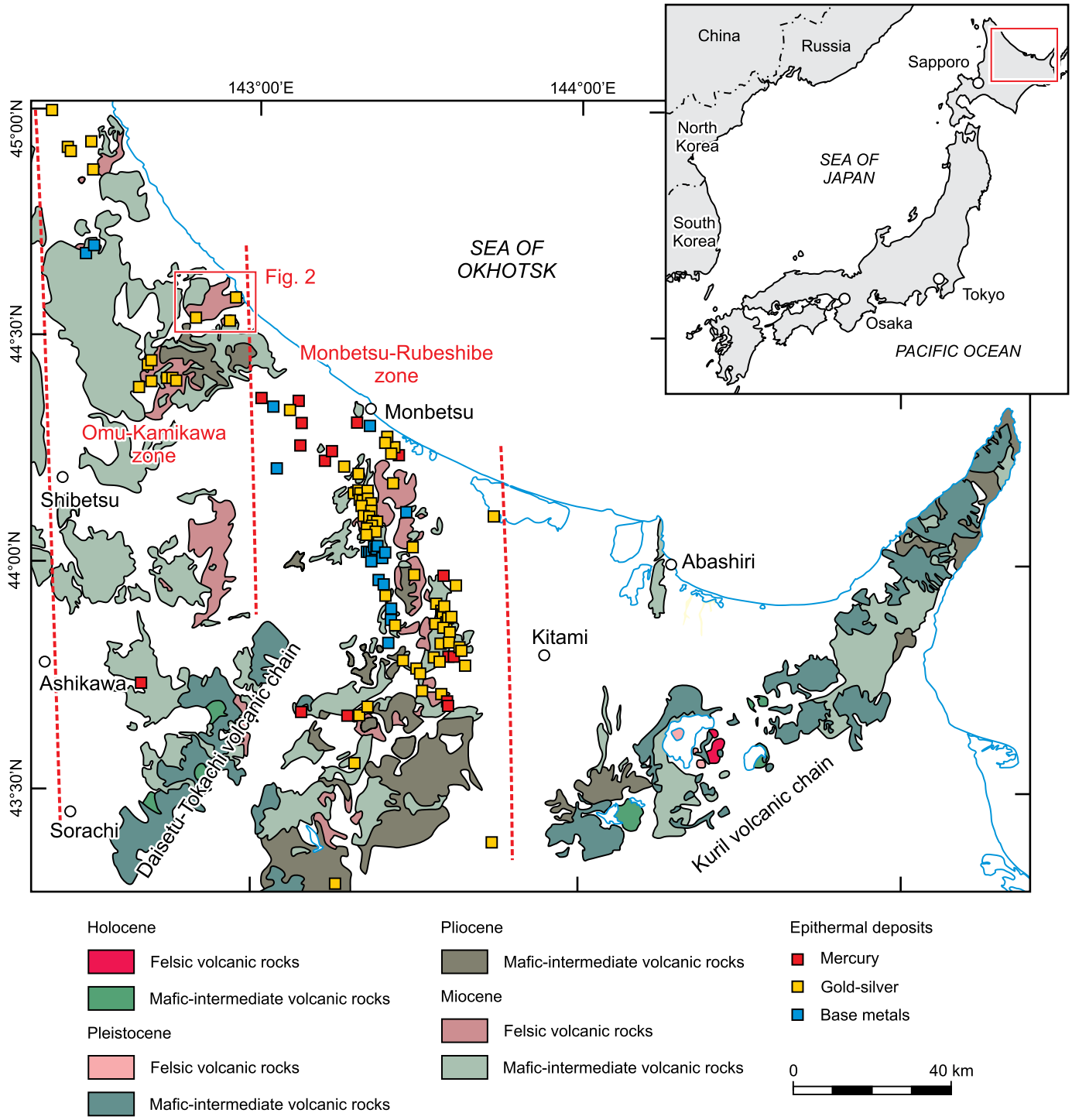

Fig. 1. Geologic setting of low-sulfidation epithermal deposits in the Kitami region of northeastern Hokkaido, Japan. Deposits occur in the Omu-Kamikawa and Monbetsu-Rubeshibe extensional zones (based on the 1:50,000 and 1:200,000 geologic map series of the Geological Survey of Japan).

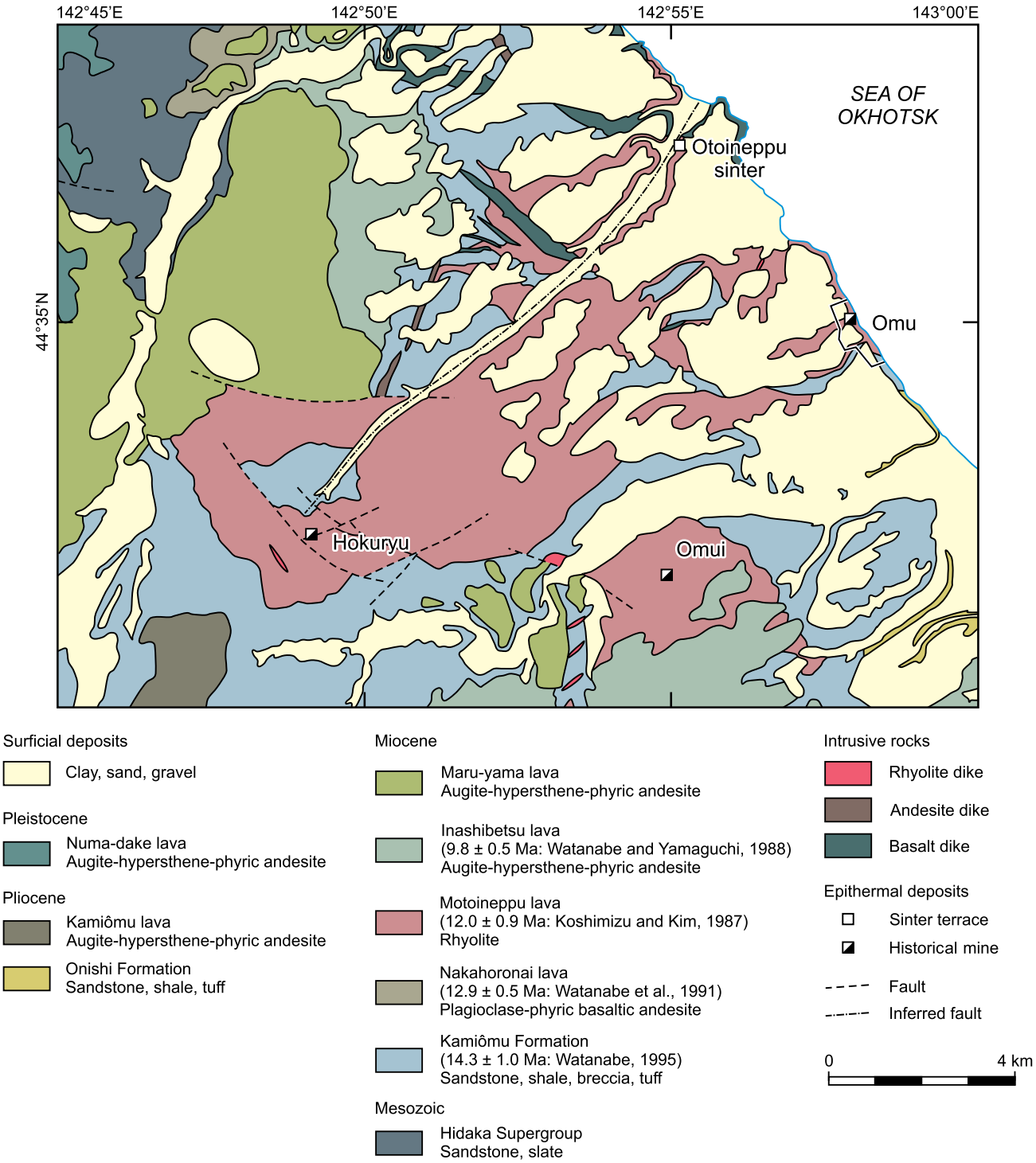

Fig. 2. Geologic map of the Omu camp showing the locations of the Omui, Hokuryu, and Omu low-sulfidation epithermal deposits. The Otoineppu sinter occurs along an inferred NE-trending fault (modified from Suzuki et al., 1966).

150 m, a downdip extent of 80 m, and an average thickness of 0.88 m. The second vein had a strike of 60°, dipped at 80° to the northwest, with a strike length of 60 m, a downdip extent of 80 m, and an average thickness of 0.60 m. Total production at Omu is estimated to have been 650 oz Au and 5,500 oz Ag (Barrett et al., 2018).

A large sinter terrace, referred to as the Otoineppu sinter, is located northwest of the town of Omu (Fig. 2). The sinter crops out over a strike length of at least 1 km and forms a small ridge that is up to 10 m in height, paralleling an inferred NE-trending fault. A sulfide-bearing sample from the base of the outcrop area assayed 14.6 g/t Au and 50.8 g/t Ag with

676 ppm As, 1,675 ppm Sb, 93 ppm Se, and >100 ppm Hg (Irving Resources, press release September 21, 2017). Artisanal mining of the Otoineppu sinter is conducted for use in landscaping in the Omu area. Recent drilling below the sinter terrace has revealed the presence of a large zone of brecciated vein material characterized by continuous Au and Ag grades. Drilling intercepted high-grade vein material, including 119 g/t Au and 1,410 g/t Ag over 0.32 m, 29.8 g/t Au and 576 g/t Ag over 1.33 m, and 12.9 g/t Au and 44.1 g/t Ag over 2.03 m (Irving Resources, press releases May 6, 2019, June 13, 2019, November 5, 2019, and April 21, 2020). Core recovered from one drill hole suggests that the volcanic rocks hosting the breccia zone is underlain by sedimentary rocks of the Mesozoic Hidaka Supergroup. A loop electromagnetic survey also suggests the occurrence of basement rocks below the drilled target (Irving Resources, press release June 13, 2019).

Materials and Methods

The present study used samples of epithermal vein material from the Omu camp collected in 2016 to 2019. Sampling was conducted from vein float and outcrop at the historic Omui and Hokuryu mines. In addition, drill core samples were collected from high-grade breccia and vein intercepts below the Otoineppu sinter. One-half of each sample was used for whole-rock geochemical analysis by ALS in Reno, Nevada (Table 1). Multielement analysis was performed by inductively coupled plasma-mass spectrometry following four-acid digestion. Silver was analyzed by this method at concentrations <100 ppm. At concentrations between 100 and 1,500 ppm, the Ag content was determined by inductively coupled plasma-atomic emission spectroscopy following four-acid digestion. At even higher concentrations, Ag was measured by fire assay with a gravimetric finish. Gold analyses were performed by fire assay with a gravimetric finish.

The distribution of precious metals in hand specimen was determined using a Bruker M4 Tornado μXRF spectrometer equipped with dual 30-mm^2 silicon drift detectors, located at the Colorado School of Mines, Colorado. The instrument was equipped with an Rh X-ray tube with polycapillary optics achieving a spot size of ~25 μm. Measurements were made under vacuum (~20 mbar) at 50 kV and 600 μA. An Al (100 μm)-Ti (50 μm)-Cu (25 μm) multilayer filter was used. Mapping was conducted along ~2-cm-wide traverses perpendicular to the vein walls at a step size of 50 μm and a data acquisition dwell time of 50 ms (equivalent to a stage speed of ~1 mm/s). The maps obtained were used to identify the mineralized colloform bands in hand specimen and to target subsampling for the preparation of thick (60 μm) polished sections for petrographic analysis. The thick sections were studied by optical microscopy in transmitted and reflected light using an Olympus BX51 microscope.

The ore mineralogy of the vein samples was studied using a TESCAN MIRA3 LMH Schottky field emission-scanning electron microscope equipped with a single-crystal YAG backscatter electron detector. Imaging was performed at a working distance of 10 mm and an accelerating voltage of 15 kV. Semiquantitative chemical analyses of minerals were performed by energy-dispersive X-ray spectroscopy using an attached Bruker XFlash 6|30 silicon drift detector. Fully quantitative compositions of ore minerals were determined by electron microprobe analysis using a JEOL JXA 8900 electron microprobe at the U.S. Geological Survey in Denver, Colorado, which is equipped with five wavelength dispersive X-ray spectrometers. Operating conditions included an accelerating voltage of 20 keV and a beam current of 20 nA, measured on the Faraday cup. A focused electron beam was used. The concentrations of Ag, As, Au, Bi, Co, Cu, Fe, Hg, Ni, Pb, S, Sb, Se, Te, and Zn were measured in the ore minerals.

Results

Vein textures

Vein samples from the Omu camp are massive, crustiform, or brecciated (Table 1). Most bonanza-grade samples are crustiform and consist of successive, narrow bands of quartz with individual bands having different colors, textures, grain sizes,

Table 1. List of Samples from the Low-Sulfidation Epithermal Deposits of the Omu Camp Investigated in This Study

Sample	Latitude	Longitude	Location	Description	Macroscopic texture	Number of sections
16OM-002	44°32.135'N	142°54.398'E	Omui	Vein float	M	2
16OM-012	44°32.155'N	142°54.454'E	Omui	Outcrop of Honpi vein	B	5
16OM-021	44°32.160'N	142°54.451'E	Omui	Vein float	C	2
16OM-024	44°32.170'N	142°54.453'E	Omui	Vein float	C	7
16OM-061	44°31.749'N	142°54.946'E	Omui	Vein float	M	1
16OM-064	44°32.145'N	142°54.581'E	Omui	Vein float	B	1
16OM-087	44°32.740'N	142°48.458'E	Hokuryu	Vein float	C	2
16OM-088	44°32.707'N	142°48.431'E	Hokuryu	Vein float	C	4
16OM-093	44°32.728'N	142°49.044'E	Hokuryu	Vein float	C	3
16OM-107	44°31.772'N	142°54.695'E	Omui	Vein float	M	1
16OM-116	44°32.186'N	142°54.683'E	Omui	Vein float	M	1
16OM-131	44°31.749'N	142°54.946'E	Omui	Vein float	M	1
16OM-132	44°31.749'N	142°54.946'E	Omui	Vein float	M	1
17OM-001	44°32.701'N	142°48.427'E	Hokuryu	Vein float	C	5
19OM-001	44°37.236'N	142°54.882'E	Otoineppu	Drill hole 19OMS-002 (184.93–185.25 m)	C	3
19OM-002	44°37.236'N	142°54.882'E	Otoineppu	Drill hole 19OMS-002 (185.25–185.72 m)	B	1
19OM-003	44°37.164'N	142°54.909'E	Otoineppu	Drill hole 19OMS-004 (311.30–311.70 m)	C	1
19OM-004	44°37.176'N	142°54.875'E	Otoineppu	Drill hole 19OMS-005 (308.93–310.30 m)	B	1

Abbreviations: B = vein breccia, C = crustiform, M = massive

and thickness (Fig. 3a-c). The bands are typically subparallel and range in thickness from about 1 to 5 mm. Many of the bands are colloform and consist of fine-grained quartz. The outer surfaces of these colloform bands exhibit botryoidal shapes. The colloform bands are white to dark gray and black, with many being yellowish, greenish, slightly pink, or tan. In addition to colloform bands, the crustiform banded vein samples also contain bands composed of bladed calcite that is replaced by quartz (Fig. 3a, c) and centerlines composed of comb quartz.

Brecciated vein material can contain high precious metal grades, especially in one prominent outcrop of breccia at the Honpi vein of the Omui deposit. At this location, high-grade breccias are composed of small banded clasts of quartz that range from several millimeters to centimeters in size (Fig. 3d). The clasts are tan, dark gray, or black and are subrounded or subangular. In addition to vein fragments, wall-rock clasts are locally present. The cement surrounding the clasts is commonly lighter in color and often appears milky white and banded, having a cockade texture in hand specimen. Vugs are common and are usually filled either with drusy quartz or with clay minerals. Bladed calcite that is replaced by quartz is sometimes present in the vugs and the matrix between the clasts.

Whole-rock geochemistry

Whole-rock geochemical data shows that massive vein samples collected in the Omu camp typically contain low precious metal grades, whereas crustiform vein samples contain up to 118.5 ppm Au and 1,410 ppm Ag (Tables 1, 2). The brecciated material from the Honpi vein of the Omui deposit is characterized by grades of 480 ppm Au and 9,660 ppm Ag. In general, samples enriched in Au also show elevated Ag concentrations (Fig. 4a). The Ag content of the vein material correlates with the whole-rock Se content (Fig. 4b). In contrast to Se, the Te content of the samples is typically <1 ppm (Table 2). The concentrations of other metals are not correlative with each other and are generally low in the samples investigated. Elevated concentrations of As (up to 640 ppm), Cu (up to 204 ppm), Pb (up to 78.2 ppm), Sb (up to 782 ppm), and Zn (up to 98 ppm) are present in some of the samples (Table 2).

Distribution of ore minerals

Chemical mapping using μXRF revealed that ore minerals are heterogeneously distributed at the hand specimen scale (Fig. 5). Ore minerals occur in specific colloform bands within the crustiform veins or are irregularly distributed between the

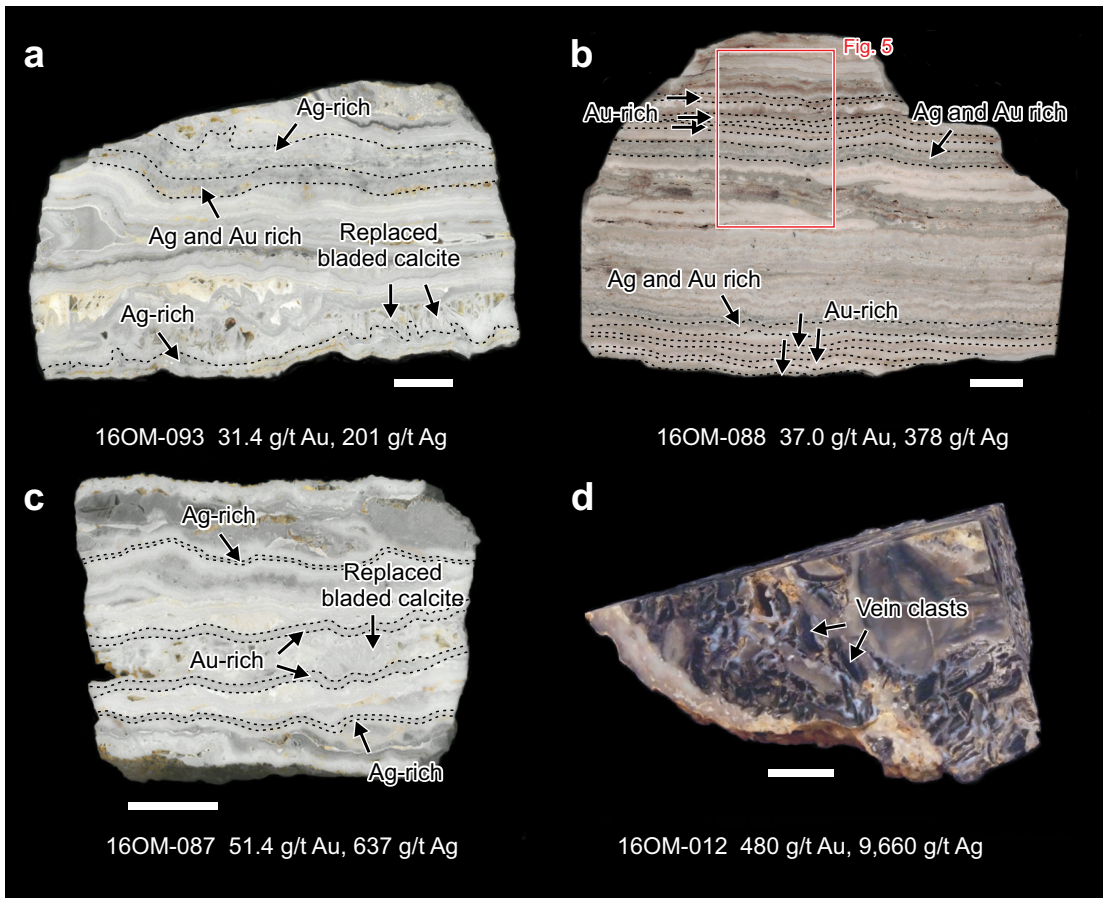

Fig. 3. Examples of vein specimens from the low-sulfidation epithermal deposits of the Omu camp. a. Crustiform vein from Hokuryu containing Au- and/or Ag-rich colloform quartz bands as well as bands of bladed calcite replaced by quartz. b. Sample of a colloform vein from Hokuryu. Ore minerals are present in colloform bands that are either Au or Ag rich. c. Crustiform vein from Hokuryu containing distinct bands that are Au or Ag rich. Bladed calcite is replaced by quartz. d. Breccia sample from the Honpi vein at Omui consisting of black vein clasts that can be Au or Ag rich. The locations of mineralized bands in the crustiform vein samples were determined by μXRF mapping. Scale bars are 2 cm.

Table 2. Trace Element Composition of Samples from the Low-Sulfidation Epithermal Deposits of the Omu Camp Investigated in This Study (in ppm)

Sample	Au	Ag	As	Bi	Cd	Cu	Pb	Sb	Se	Te	Zn
16OM-002	2.86	10.2	62.5	0.03	<0.02	6.3	4.6	71.6	1	0.05	<2
16OM-012	480	9,660	88.5	0.02	0.09	19.6	33.2	360	415	<0.05	2
16OM-021	48.2	1,030	25.2	0.02	0.02	15.5	6.4	81.7	40	0.26	2
16OM-024	67.6	1,060	17.9	0.03	0.03	15.9	7.8	98.1	39	0.65	<2
16OM-061	<0.05	1.45	5.7	0.03	<0.02	1.2	1.4	394	<1	<0.05	<2
16OM-064	10.7	107	5.9	0.04	<0.02	3.4	2.5	23.9	10	0.50	4
16OM-087	51.4	637	67.2	6.54	0.03	12.1	15.8	132	57	0.09	5
16OM-088	37.0	378	5.7	2.22	<0.02	2.6	5.6	54.2	42	0.15	3
16OM-093	31.4	201	34.2	1.88	<0.02	3	14.3	59.3	27	0.63	2
16OM-107	0.11	1.50	0.5	0.15	<0.02	2.7	4.5	220	1	<0.05	2
16OM-116	1.92	35.5	4.97	0.19	<0.02	18.5	11.9	29.8	6	0.06	4
16OM-131	<0.05	11.5	60.1	0.36	0.06	6.3	46.2	307	2	<0.05	37
16OM-132	<0.05	4.06	11.3	0.23	0.07	11.3	28.6	782	1	<0.05	23
17OM-001	56.0	707	16.2	4.08	0.13	15.7	78.2	71.1	78	0.16	61
19OM-001	118.5	1,410	425	0.35	0.41	204	11.1	511	297	0.55	71
19OM-002	1.61	629	161	0.08	0.11	21.1	6.0	273	93	0.16	86
19OM-003	2.34	34.5	640	0.02	0.05	261	4.5	184	41	1.01	98
19OM-004	17.8	59.4	159	0.24	0.11	444	9.5	81.7	9	0.63	54

clasts and matrix of brecciated samples. In many of the crustiform vein samples, enrichment in Au and Ag occurs in different colloform bands, although both precious metals can also occur in elevated concentrations in the same bands.

Colloform bands that contain elevated Au contents are typically light gray to white in color (Fig. 5). The bands are macroscopically similar to other bands in the crustiform veins that are barren. In contrast, high Ag contents occur in dark-gray to black colloform bands that contain opaque minerals visible with a hand lens. Elevated Ag concentrations correlate with an enrichment in Se. Some dark-gray to black colloform bands contain elevated Au contents, whereas others do not.

Quartz textures

Based on optical microscopy, a number of distinctive quartz textures were identified in the vein samples from the Omu camp using the textural classification schemes developed by Adams (1920), Bobis (1994), Dong et al. (1995), Etoh et al. (2002), Moncada et al. (2012), and Shimizu (2014). Textures identified included primary textures such as comb and zonal quartz; textures formed through recrystallization such as feathery, flamboyant, and ghost-sphere quartz; and textures formed through replacement of other gangue minerals such as calcite and adularia, which includes lattice-bladed, ghost-bladed, parallel-bladed, radiating-bladed, and saccharoidal quartz. Emphasis was placed on the microscopic investigation

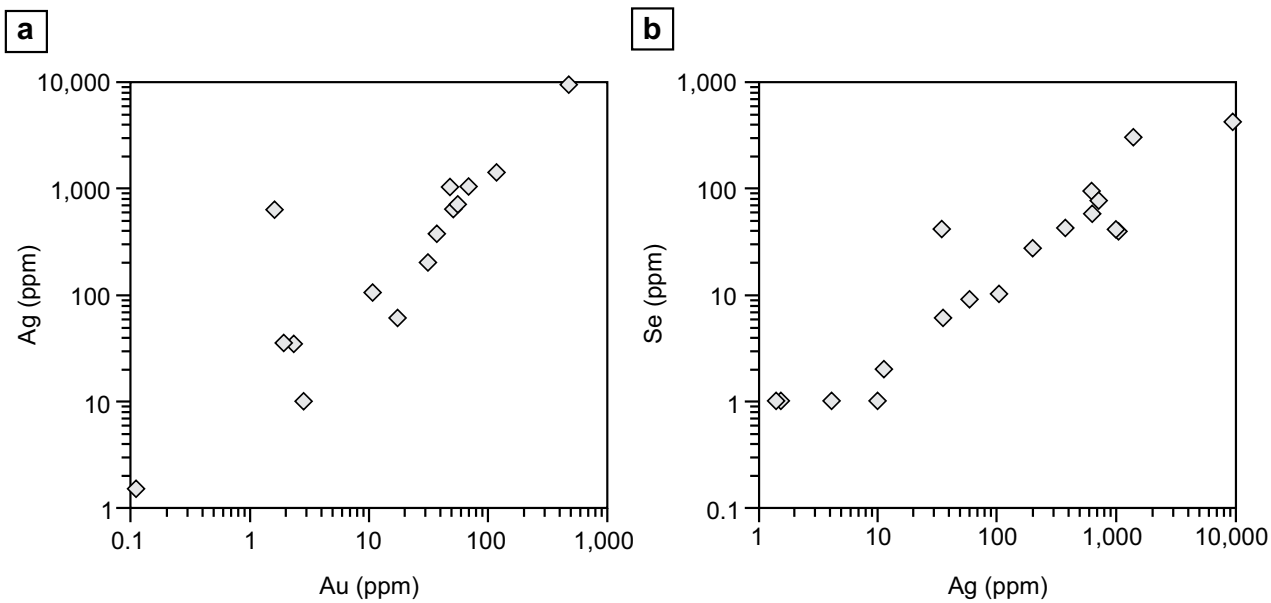

Fig. 4. Trace element geochemistry of quartz vein samples from the Omu camp. a. The precious metal grades of the samples broadly correlate, although Au and Ag do not necessarily occur in the same colloform bands. b. The Ag and Se contents of the samples correlate, which is consistent with the microscopic observation that Ag sulfoselenides are abundant in some colloform bands.

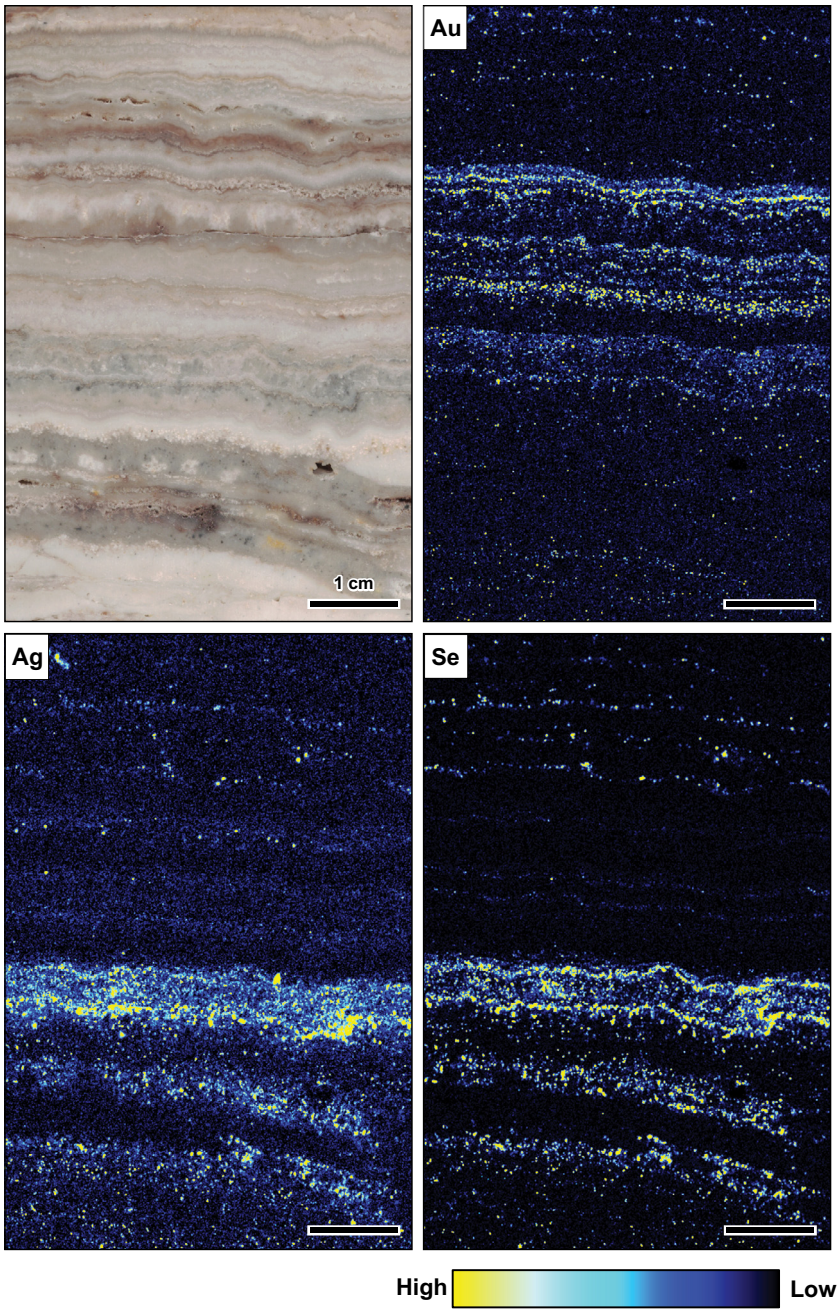

Fig. 5. Sample image and corresponding trace element maps of a representative crustiform quartz vein sample from the Omu camp. The element maps show that only some of the colloform bands that are characterized by Au enrichment also show elevated Ag contents. In contrast, the distributions of Ag and Se are similar. The maps were obtained by μXRF mapping of a portion of specimen 16OM-088 shown in Figure 3b.

of the colloform bands, as μXRF mapping showed that ore minerals almost exclusively occur within these bands. High-magnification optical microscopy revealed that three texturally distinct types of colloform quartz can be distinguished.

Samples with high precious metal grades contain microspherical colloform quartz (Fig. 6), which is interpreted to represent a primary quartz texture (cf. Sherlock and Lehrman, 1995; Taksavasu et al., 2018). At high magnifications, microspheres having sizes $\lesssim 5\,\mu$m can be recognized in plane-polarized light (Fig. 6a, b). The microspheres locally form globular aggregates that can reach up to 20 to 50 μm in size. In some areas, relic microspheres can be recognized, whereas in others they are fused to form microcrystalline quartz with a mosaic texture (Fig. 6c). Cavities between the microspheres can show sickle-like shapes outlining the relic microspheres. The proportion of voids in the microspherical colloform quartz is typically high, giving the quartz a dark-gray to brown color in transmitted light. In crossed-polarized light, the microspherical colloform bands consist of microcrystalline quartz with a mosaic texture (Fig. 6d). The microspherical colloform quartz bands lack fluid inclusions, precluding use of any inclusions for determining the original formation conditions of the colloform bands.

In addition to the microspherical colloform quartz, ore samples contain bands of chalcedonic colloform quartz that is composed of chalcedonic fibers oriented perpendicular to the colloform bands (Fig. 7). Where tested, the chalcedonic fibers

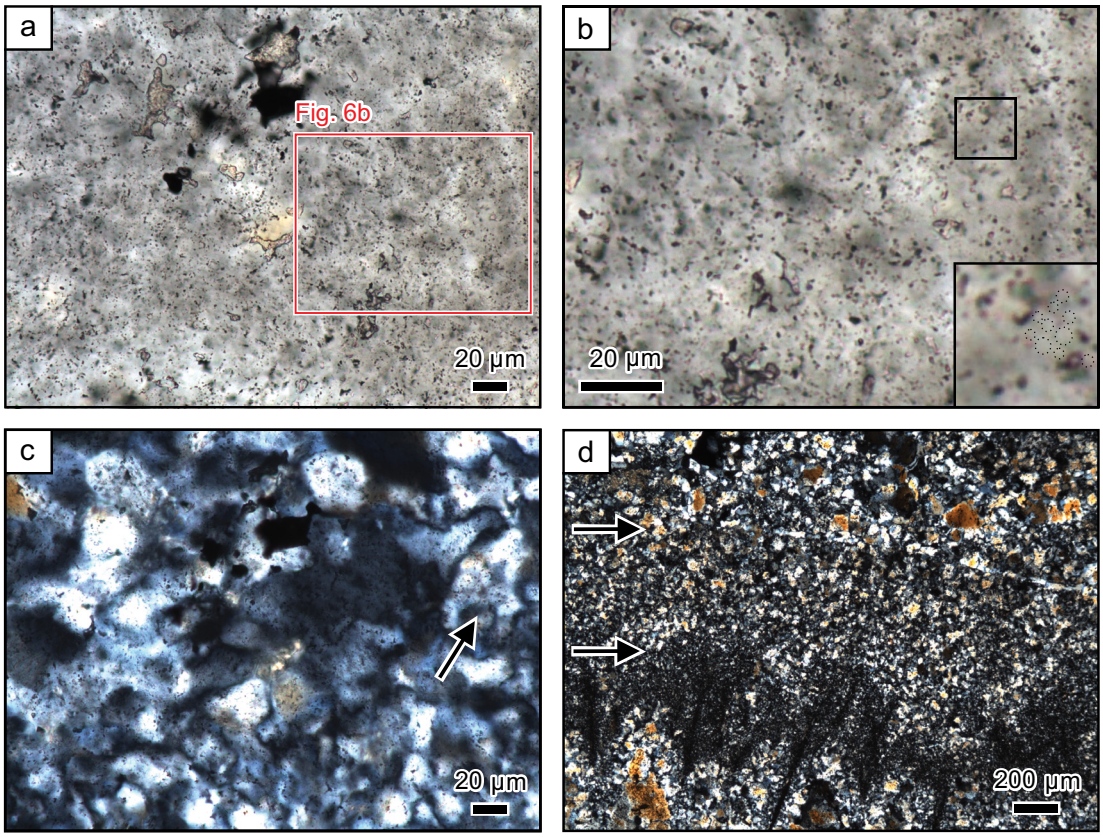

Fig. 6. Photomicrographs of microspherical colloform quartz textures present in vein samples from the Omu camp. a. Plane-polarized light image of quartz showing a remnant texture of spherical aggregates. Small spherical aggregates can be recognized. Sample 16OM-002. b. High-magnification plane-polarized light image showing textures interpreted to be relic microspheres. Location of the image is shown in Figure 6a. A higher magnification image of one location with abundant relic microspheres is given as an inset. Note that the relic microspheres are only 1 to 3 μm in size. The outlines of selected microspheres are highlighted. c. Crossed-polarized light image of the same field of view as Figure 6a showing textures interpreted to be an example of microspherical quartz recrystallized to mosaic quartz. The arrow points to the area with relic microspheres shown as an inset in Figure 6b, which is now characterized by the presence of small anhedral quartz grains formed through recrystallization. d. Low-magnification crossed-polarized light image showing a band of fine-grained mosaic quartz confined by botryoidal surfaces (arrows). The band below the mosaic quartz contains ghost blades. Sample 17OM-001.

are length-fast. Alternating bands of chalcedonic fibers have variable thicknesses ranging up to 100 μm (Fig. 7a-c). Under crossed-polarized light, the chalcedonic colloform quartz shows radial or flamboyant extinction patterns. This type of colloform texture also lacks fluid inclusions. The chalcedonic colloform quartz does not contain ore minerals.

Many of the colloform quartz bands in the samples from the Omu district are composed of microcrystalline quartz exhibiting a mosaic texture in crossed-polarized light (Figs. 6c, d, 7d). Different degrees of development of mosaic texture have been identified, demonstrating that this texture can form through recrystallization from the microspherical colloform quartz (Fig. 6c, d) and the chalcedonic colloform quartz (Fig. 7d). Where intensely recrystallized, the quartz grains have polygonal shapes. In cases of less intense recrystallization, the boundaries of adjacent mosaic quartz grains are not well defined, leading to a mottled appearance. In some cases where the mosaic quartz has formed through recrystallization of microspherical colloform quartz, the locations of the interpenetrating grain boundaries in the mosaic quartz appear to be controlled by the presence of former globular aggregates. Where the mosaic quartz formed from chalcedonic quartz, the bands of coarse-grained mosaic quartz sometimes host moss and ghost-sphere textures consisting of remnant chalcedonic fibers.

Textural setting of ore minerals

In the bonanza-grade vein samples from the Omu camp, ore minerals primarily occur in specific colloform bands (Figs. 3, 5). To quantify the relationship between the ore minerals and quartz textures, thick sections from 15 samples were investigated. Transects were drawn across each slide, approximately perpendicular to the vein walls, to include as many different quartz textures as possible. Subsequently, the different quartz types occurring along the traverses were documented. The occurrence of ore minerals along the transects was determined by optical microscopy using reflected light. Point counting of ore mineral grains was conducted within an envelope of ~4 mm along the transects. Complexly intergrown grains were treated as a single occurrence during point counting. In addition to the point counting, μXRF mapping was conducted along the traverse to quantify the relative proportions of Au,

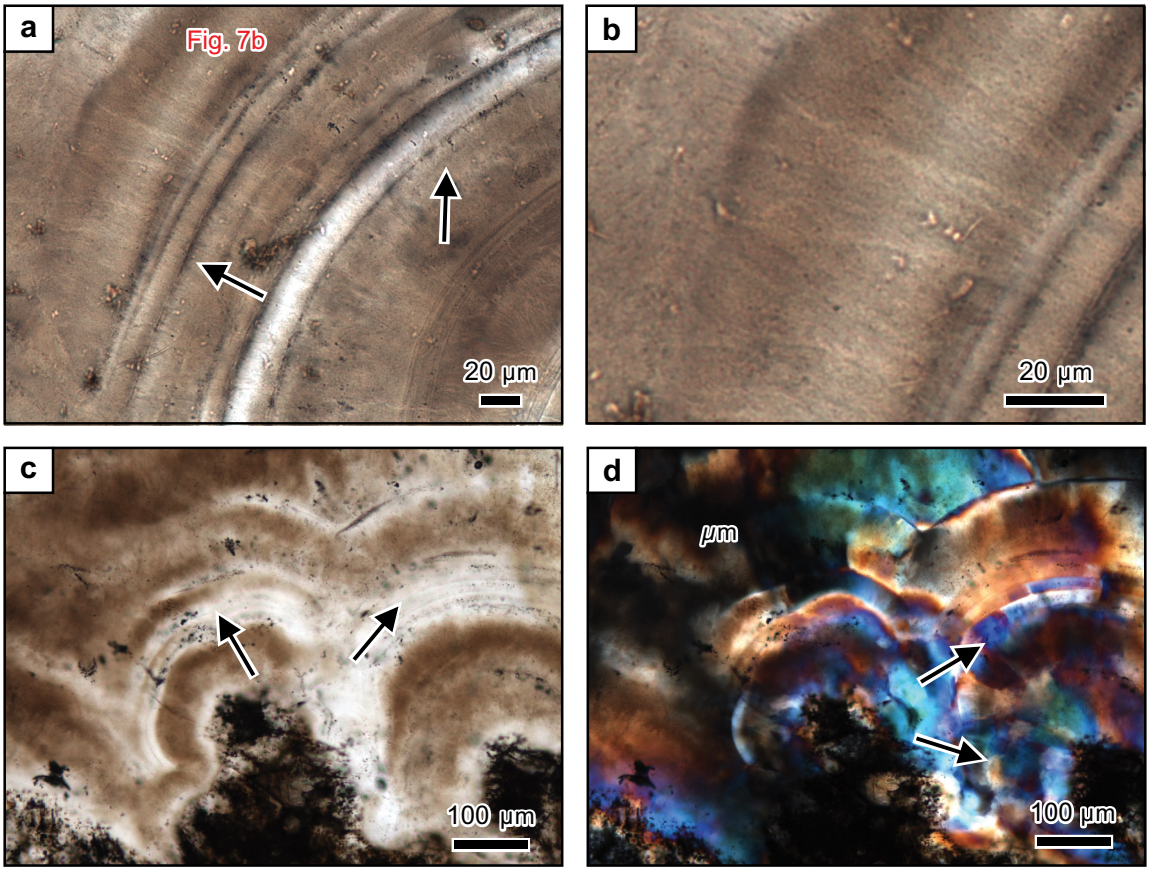

Fig. 7. Photomicrographs of chalcedonic colloform texture present in vein samples from the Omu camp. a. Plane-polarized light image showing chalcedonic fibers (arrows). b. High-magnification image of the chalcedonic fibers. Location of the image is shown in Figure 7a. c. Low-magnification plane-polarized light image of chalcedonic colloform bands (arrows). d. Corresponding crossed-polarized light image showing the partial recrystallization of chalcedonic colloform bands to mosaic quartz (arrows). Sample 16OM-012.

Ag, and Se present in the different bands and to ensure that all bands containing ore minerals were correctly identified by optical microscopy. Relative element concentrations, given as total X-ray counts, were produced from the μXRF element maps by integrating at each pixel step the count data from 35 pixels perpendicular to and on either side of the traverse line. An example of one of the traverses conducted is given in Figure 8.

In total, the textural locations of ~1,000 ore mineral grains were determined in the 15 samples. Of those, 70% were located within colloform quartz bands showing clearly identifiable relic microspheres, and 30% were located in mosaic quartz containing no visible microspheres. In transmitted light, the ore minerals are finely distributed throughout these quartz bands (Fig. 9). Only a few ore minerals were recognized in bands having other quartz textures. Most notably some electrum grains are present in bands of lattice-bladed quartz that formed by replacement of calcite.

Mineralogy of ore and opaque minerals

Most of the electrum occurs as small complexly shaped grains or wiry aggregates in the colloform bands, many of which show relic microspheres. The electrum infills pore space between microspheres, with the electrum typically being in direct contact with the relict microspheres (Fig. 9b). Electrum grains are golden to whitish in reflected light and range from 15 to 40 μm in size. The electrum has a millesimal fineness of 421 to 616 (Fig. 10). Electron microprobe analysis of a representative subset of grains revealed that the Hg concentrations of the electrum are low (<0.5 wt %, n = 12). The other elements analyzed were typically below detection limit.

Sulfoselenides represent the principal host to Ag in the samples investigated. In reflected light, the Ag sulfoselenides are light gray, very weakly anisotropic, and sometimes have a greenish cast. They have a low reflectance with a metallic or adamantine luster. The Ag sulfoselenides form irregularly shaped grains that range in size from <10 to 120 μm. They are in direct contact with the microspheres or, more commonly, with small, euhedral quartz crystals that may have formed through recrystallization of the microspheres (Fig. 9c, d). The recrystallized quartz showing a mosaic texture in crossed-polarized light frequently contains encapsulated Ag sulfoselenides (Fig. 9d). The Ag sulfoselenides can be intergrown with minor electrum and uytenbogaardtite (Ag_3AuS_2). Microanalysis showed that Ag sulfoselenides in the Omu camp belong to the solid solution between acanthite and naumannite (Fig. 11). Electron microprobe analyses revealed that Se-bearing acanthite typically contains elevated Sb concentrations (up to 9.36 wt %, n = 38).

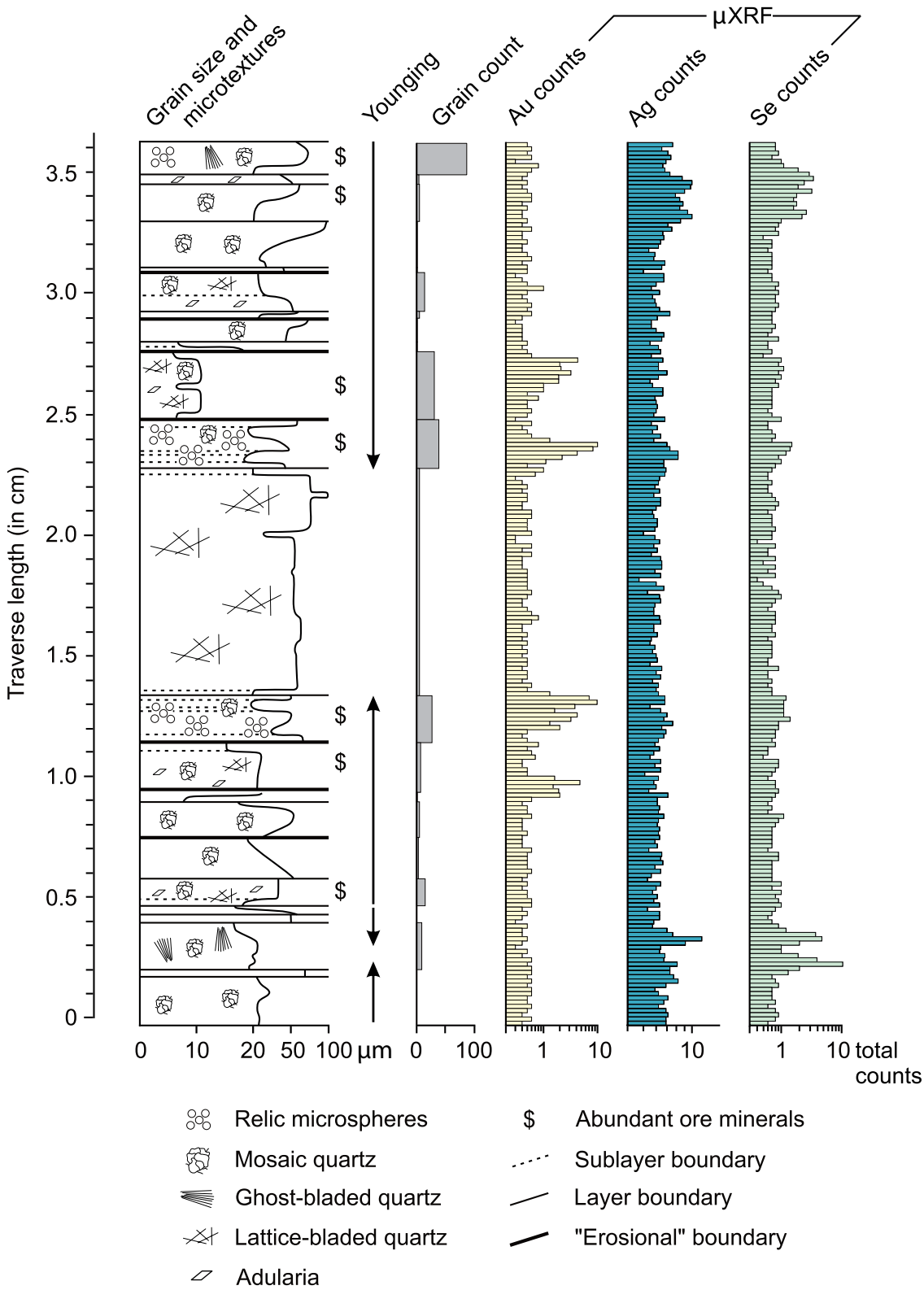

Fig. 8. Representative traverse across a crustiform quartz vein sample from the Omu camp recording the occurrence of different quartz microtextures and the distribution of ore minerals. The diagram shows that electrum and Ag sulfoselenides occur preferentially in certain colloform bands. These bands show a mosaic texture, and some of the mineralized bands contain relic microspherical textures. Sample 16OM-87.

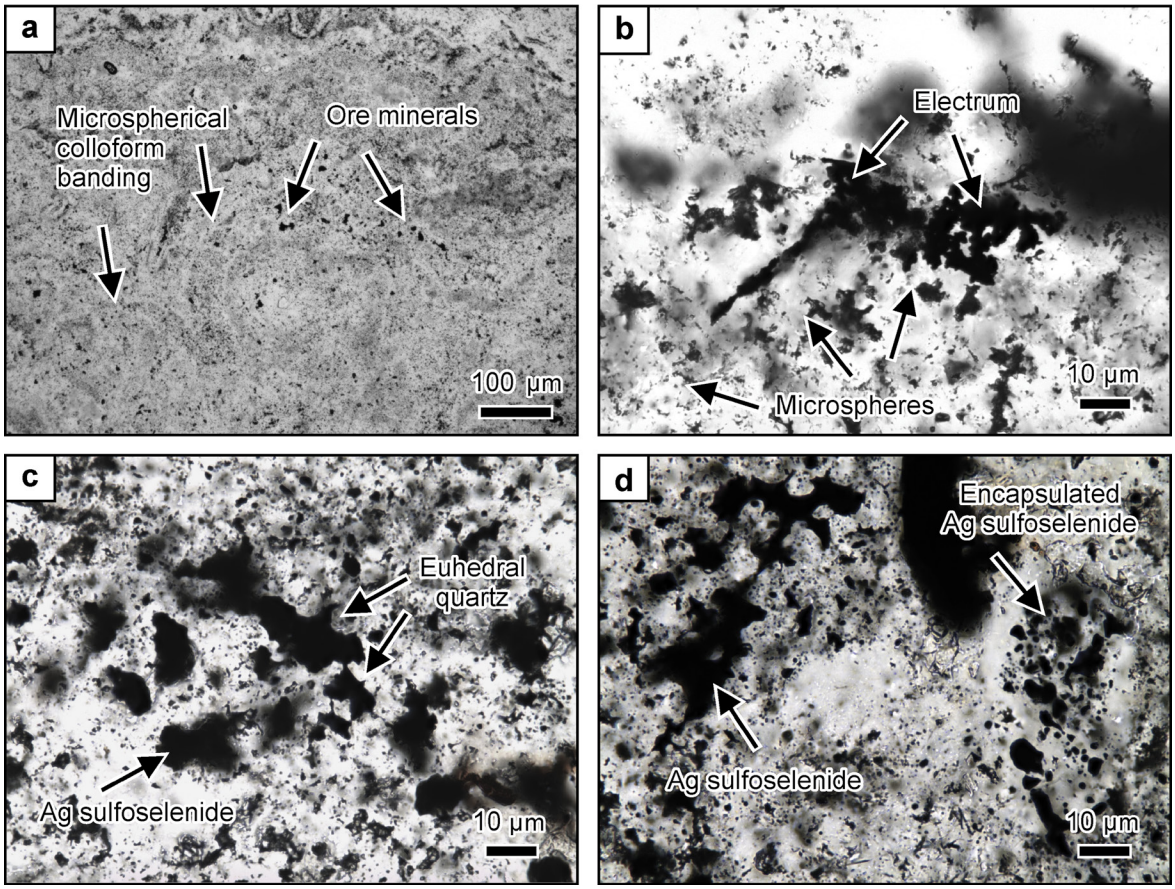

Fig. 9. Photomicrographs showing ore minerals within microspherical colloform banding in bonanza-grade samples from the Omu camp. a. Low-magnification plane-polarized light image showing a microspherical colloform quartz band. Sample 17OM-001. b. High-magnification image of a wiry aggregate of electrum occurring in a microspherical colloform band. The electrum is in direct contact with relic microspheres. Sample 16OM-087. c. High-magnification image of Ag sulfoselenide grains in a colloform band showing mosaic texture. The originally microspherical matrix is recrystallized, and small euhedral quartz crystals occur in contact with the opaque phases. Sample 17OM-001. d. High-magnification image of Ag sulfoselenide present in a colloform band showing mosaic texture. The ore minerals are in contact with small euhedral quartz crystals. Some of the quartz contains encapsulated Ag sulfoselenides. Sample 17OM-001.

Pyrite is rare and is only abundant in some of the samples from Otoineppu. Rare pyrargyrite was recognized by reflected light and scanning electron microscopy. The pyrargyrite is deep red in transmitted light and bluish gray in reflected light. Although pyrargyrite is a strongly anisotropic mineral, the carmine red internal reflections mask this property. Scanning electron microcopy further revealed the presence of trace amounts of barite, chalcopyrite, and tetrahedrite. Iodargyrite was recognized in rare cases and occurred in intergrowth with Fe-oxide/hydroxide, suggesting that this phase may be a product of surface weathering of the samples analyzed.

Discussion

Origin of quartz textures

Vein textures in low-sulfidation epithermal deposits can be primary or may have formed as a result of recrystallization and replacement processes (Bobis, 1994; Dong et al., 1995; Etoh et al., 2002; Moncada et al., 2012). Primary textures are formed through growth of quartz crystals into open space or direct precipitation of silica from hydrothermal solutions. Recrystallization textures form through the transition from a metastable silica precursor to thermodynamically stable quartz. Replacement textures are partial or complete pseudomorphs of earlier formed gangue minerals, such as calcite and adularia, by quartz.

Previous workers have emphasized that colloform textures (Rogers, 1917) in low-sulfidation epithermal deposits are typically of primary origin (Bobis, 1994; Dong et al., 1995; Sherlock and Lehrman, 1995; Moncada et al., 2012; Taksavasu et al., 2018). The petrographic investigations of this study show that different types of colloform textures that form by contrasting mechanisms can be distinguished. The microspherical and chalcedonic colloform textures are undoubtedly of primary origin. However, the colloform bands composed of mosaic quartz could have formed through recrystallization of both types of primary textures.

The microspherical colloform texture is typified by the presence of relic microspheres or globular aggregates of fused microspheres. This type of colloform banding has been previously recognized by Sherlock and Lehrman (1995) at the McLaughlin deposit in California and by Taksavasu et al.

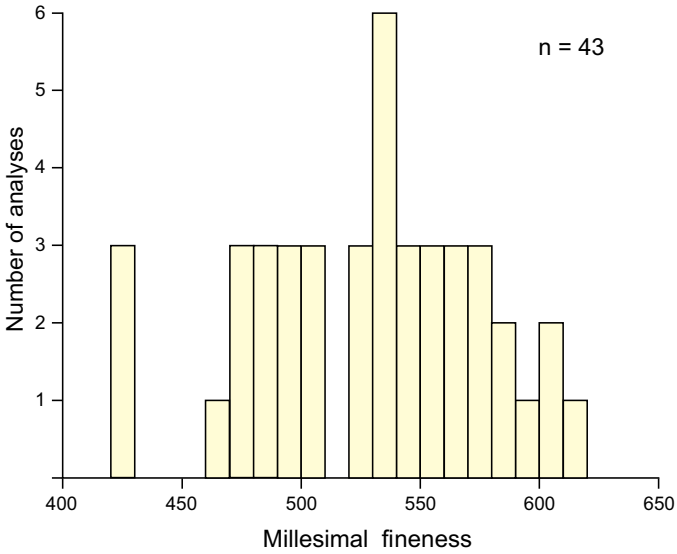

Fig. 10. Millesimal fineness of electrum contained in low-sulfidation epithermal vein samples from the Omu camp. Compositional analyses were conducted on the electron microprobe and by scanning electron microscopy.

(2018) at Buckskin National in Nevada. The microspheres in the colloform bands are interpreted to have been originally composed of noncrystalline silica that was directly deposited from hydrothermal solutions. In crossed-polarized light, the microspherical colloform bands in the samples from the Omu camp consist of microcrystalline quartz exhibiting a mosaic texture, suggesting that the noncrystalline silica precursor phase has entirely recrystallized to quartz subsequent to deposition. Textural maturation appears to have resulted in the formation of increasingly larger quartz grains having interpenetrating grain boundaries.

In contrast, the chalcedonic colloform texture consists of microcrystalline fibrous quartz. Chalcedony is common in crustiform veins and has been reported from many low-sulfidation epithermal deposits (Sander and Black, 1988; Bobis, 1994; Dong et al., 1995). The texture consists of rhythmic bands composed of radiating chalcedonic fibers that are oriented perpendicular to the substrate on which the bands have developed, which includes euhedral quartz crystals. The outermost bands form botryoidal surfaces in open space, suggesting that the colloform bands are a primary texture formed from a hydrothermal solution. The microcrystalline fibers in the chalcedonic colloform bands consist of quartz crystals that are predominately length-fast with their crystallographic c-axes being oriented perpendicular to the long axes of the fibers (cf. Miehe et al., 1984). The fibrous nature of the quartz can be readily identified and is texturally distinct from the microspherical colloform texture. Flamboyant extinction patterns are common in this type of colloform banding, as described by Sander and Black (1988) and Dong et al. (1995). The chalcedonic colloform banding can also recrystallize to mosaic quartz. The flamboyant extinction pattern seen in crossed-polarized light sometimes contains mosaic texture, while in other areas, mosaic quartz composed of coarse grains contains relic fibers, which may still be recognized in plane-polarized light.

Lovering (1972) proposed that mosaic quartz forms through recrystallization. Textural evidence from this study shows that coarse-grained mosaic quartz can form through the recrystallization of both the microspherical and the chalcedonic colloform textures. In some cases, transitions from the preexisting colloform banding can be observed, including relic microspheres or fibrous quartz. However, in bands where complete recrystallization to mosaic quartz occurred, the precursor textures cannot be identified with optical microscopy.

Gangue mineral textures and distribution of ore minerals

The detailed microtextural studies along traverses show conclusively that ore minerals are present primarily in the microspherical colloform quartz and in mosaic quartz formed through recrystallization of the microspheres (Fig. 8). Only minor electrum was detected in other quartz textures such as lattice-bladed quartz. Most notably, the chalcedonic colloform bands and mosaic quartz that formed through recrystallization of this primary texture are barren.

This finding is consistent with previous studies establishing that ore minerals in low-sulfidation epithermal veins are mostly hosted by colloform quartz bands, although the different types of primary colloform banding distinguished here were not previously recognized. Moncada et al. (2012) studied gangue mineral textures in 855 samples from the Veta Madre in the Guanajuato region of Mexico. They identified a range of textures, including colloform quartz, plumose, feathery or flamboyant quartz, and bladed calcite replaced by quartz. They showed that colloform quartz is the most important indicator of mineralization. An average grade of 1.1 g/t Au and 178.8 g/t Ag was recorded in samples containing colloform quartz, whereas samples without colloform quartz only averaged 0.2 g/t Au and 17.2 g/t Ag (Moncada et al., 2012). Shimizu (2014) studied bonanza-grade samples from

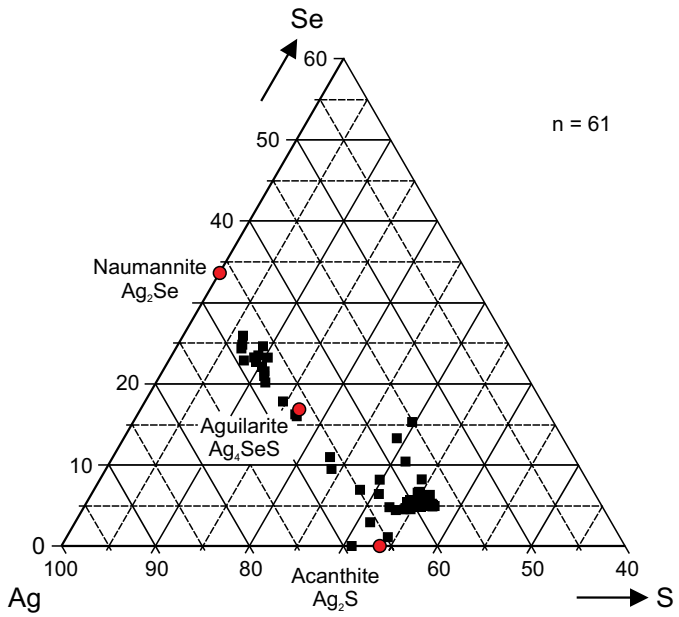

Fig. 11. Ternary diagram (in at. %) illustrating compositional variations of the Ag sulfoselenides in low-sulfidation epithermal vein samples from the Omu camp. Compositional analyses were conducted on the electron microprobe and by scanning electron microscopy.

the Koryu deposit in Japan and showed that both colloform and mosaic quartz are hosts to ore minerals. Petrographic investigations by Saunders (1990, 1994) on the Sleeper deposit in Nevada also showed that ore minerals occur in colloform quartz bands. However, he noted that the colloform quartz in the bonanza-grade veins at Sleeper is composed of alternating gold-rich and barren bands, confirming the finding of this study that not all types of colloform banding are host to ore minerals. At McLaughlin in California, Sherlock and Lehrman (1995) showed that electrum occurs as dendrites in colloform bands consisting of compacted silica microspheres that are texturally identical to the microspherical colloform bands described here. A petrographic study on vein material from Khan Krum in Bulgaria revealed that electrum dendrites in this deposit also primarily occur in colloform quartz bands (Marinova et al., 2014).

The observations on the ore samples from the Omu camp suggest that ore-mineral-bearing colloform bands with microspherical microtexture are formed by processes that differ from those forming chalcedonic colloform bands that are barren. This implies that the quartz microtextures are key to understanding the processes of ore deposition.

Noncrystalline silica precursor to microspherical colloform bands

The ore-mineral-bearing colloform bands in the vein samples from the Omu camp were originally composed of 1- to 5-μm microspheres and globular aggregates consisting of fused microspheres. The textures observed are similar to those documented in scales in high-enthalpy geothermal power operations (Rothbaum et al., 1979; Brown, 2011; Meier et al., 2014; Zarrouk et al., 2014; van den Heuvel et al., 2018) that almost exclusively consist of noncrystalline silica because quartz deposition is kinetically inhibited (Gudmundsson and Bott, 1979; Yokoyama et al., 1993; Gallup, 1997; Brown, 2011). The scaling forms as silica colloids form in the liquid agglomerate and attach to the walls of well and pipes (Brown, 2011). Silica scaling occurs in well heads, separators, pipes, turbines, and heat exchangers (Skinner et al., 1967; Karabelas et al., 1989; Akaku, 1990; Christenson and Hayba, 1995; Reyes et al., 2002; Raymond et al., 2005; Zarrouk et al., 2014; Jamero et al., 2018). Dissolution-reprecipitation processes occurring over time result in the maturation of the microspherical opal-A to paracrystalline opal-CT and quartz (Reyes et al., 2002; Raymond et al., 2005).

Silica sinters formed in modern geothermal systems also primarily consist of microspherical opal-A (Jones et al., 1997; Herdianita et al., 2000; Campbell et al., 2002; Guidry and Chafetz, 2003; Lynne and Campbell, 2004; Rodgers et al., 2004; Fernandez-Turiel et al., 2005; Taksavasu et al., 2018). Studies of silica sinters of different geologic ages have shown that the opal-A is thermodynamically unstable and matures over time. The maturation process of opal-A involves the transformation into thermodynamically more stable paracrystalline opal-CT, which in turn recrystallizes into opal-C and then into microcrystalline quartz (Herdianita et al., 2000; Campbell et al., 2001; Lynne and Campbell, 2004; Rodgers et al., 2004; Lynne et al., 2005, 2007).

Maturation of opal-A may explain why microspherical colloform bands in the samples from the Omu camp are today entirely composed of anisotropic quartz. In contrast, Saunders (1990) reported that silica in colloform bands in bonanza-grade samples from the Sleeper deposit in Nevada are still virtually isotropic, and X-ray diffraction investigations confirmed the presence of opal-CT. The degree of maturation of opal-A originally present in colloform bands in vein samples likely relates to the thermal evolution of the hydrothermal system following silica deposition. Laboratory studies demonstrate that the transformation from opal-A to quartz is temperature dependent and may occur within days to months under elevated temperature conditions (Ernst and Calvert, 1969; Bettermann and Liebau, 1975; Oehler, 1976).

Physical nature of microspherical colloform bands at the time of deposition

Saunders (1990, 1994) suggested that the ore-mineral-bearing colloform bands in low-sulfidation epithermal veins were gel-like at the time of deposition. He documented textures reminiscent of sedimentary ripple marks at the Sleeper deposit in Nevada, indicating hydraulic shaping of the material during vein formation or gravity-induced sagging of the soft silica. In addition, he observed silica clasts showing evidence for deformation in a soft state that were transported along the veins and deposited in pockets (Saunders, 1990, 1994). Saunders (1994) also described a texture, subsequently referred to as the sluice-box texture (Saunders et al., 2008, 2011), in which ore minerals intermixed with silica were deposited around protrusions of the vein walls forming a thin layer over the tops of the protrusion and a thick deposit on the leeward side. Sluice-box textures have also been recognized at Fire Creek in Nevada (Milliard et al., 2015), Hollister in Nevada (Saunders et al., 2008, 2011; Unger, 2008), Koryu in Japan (Shimizu, 2014), Republic in Washington (Saunders et al., 2011), and Silver City in Idaho (Aseto, 2012). At Omu, no conclusive textural evidence for hydraulic shaping of the ore-bearing colloform bands has been identified, which can be related to the widespread recrystallization of the originally microspherical bands to mosaic quartz.

Textural relationships between microspherical silica and ore minerals

Saunders (1990) proposed that electrum dendrites contained in colloform bands formed within open space and were precipitated together with the silica matrix surrounding the ore minerals. Saunders (1994) and Saunders and Schoenly (1995) provided textural evidence from the National and Sleeper deposits in Nevada that electrum dendrites formed topographic highs within the host colloform bands. These highs appear to have influenced subsequent silica deposition. In contrast, Sherlock and Lehrman (1995) proposed that electrum dendrites grew within the microspherical colloform bands after deposition of the host at the McLaughlin deposit in California. They suggested that the delicate intergrowth between the electrum dendrites and the silica host suggests that the microspherical silica formed a framework in which the electrum dendrite grew.

The textural evidence of this study suggests that electrum hosted by the microspherical colloform bands may have formed during or immediately after the deposition of the silica microspheres. Based on their delicate nature and the fact

that the electrum is located within the microspherical host, the electrum aggregates likely grew within the microspherical matrix. Growth of the electrum may have occurred from the hydrothermal liquid circulating through the pore space between the microspheres. Processes involved in the formation of the Ag sulfoselenides may have been similar to those involved in the growth of the electrum aggregates. However, most Ag sulfoselenides are in contact with small euhedral quartz crystals that appear to have formed as a result of recrystallization of the microspherical silica, obscuring primary textural relationships between the Ag sulfoselenides and the immediate host.

Compositional variations in microspherical colloform bands

Chemical mapping of banded vein samples from the Omu camp establishes that individual microspherical colloform bands can have variable compositions. In the samples investigated, elevated Ag contents occur in macroscopically recognizable dark-gray to black colloform bands. The occurrence of this type of band is well documented in low-sulfidation epithermal deposits. Historically, these bands are referred to as "ginguro" layers, which is the Japanese word for silver black. One of the earliest descriptions of ginguro ore bands is given by Mukaiyama (1950) for the epithermal ore of the Sado Kinzan deposit in Japan. Other deposits characterized by the occurrence of ginguro bands include Buckskin National in Nevada (Saunders et al., 2008), Ivanhoe in Nevada (Saunders et al., 2008), Koryu in Japan (Shimizu et al., 1998; Shimizu, 2014), Kushikino in Japan (Takeuchi and Shikazono, 1984), and Midas in Nevada (Leavitt et al., 2004). Some of the best examples of ginguro bands have been documented at the high-grade Hishikari deposit of Kyushu in Japan (Izawa et al., 1990; Matsuhisa and Aoki, 1994; Faure et al., 2002; Shimada et al., 2005; Sanematsu et al., 2006). At all of these deposits, ginguro bands have been regarded to be the primary host to precious metals. However, in many of the crustiform vein samples investigated, the ginguro bands are not the main host to gold. The Ag sulfoselenides in the ginguro bands are intergrown with only minor amounts of electrum and uytenbogaardtite.

In the samples from the Omu camp, high Au contents also occur in microspherical colloform bands that are light gray to white in color and contain only a low abundance of Ag sulfoselenides. In reference to their Au-rich nature, Tharalson et al. (2019) coined the term "gankin" bands for this type of colloform layer. Due to their visually inconspicuous nature, the occurrence of gankin bands is probably commonly overlooked in studies of low-sulfidation epithermal deposits, except for cases where the Au content is high enough to allow easy recognition of visible gold in hand specimen or thin sections. Possible occurrences of gankin bands include McLaughlin in California where electrum-bearing, microspherical colloform bands are characterized by an unusual amber color due to presence of hydrocarbons (Sherlock and Lehrman, 1995). At Sleeper in Nevada, gold-rich bands contain up to 50% electrum, with the silica host ranging in color from milky white, tan, brownish red, blue gray, to black (Nash et al., 1989; Saunders, 1990, 1994).

The observations of this study that precious metals preferentially occur in different microspherical colloform bands in crustiform veins have far-reaching consequences for the understanding of the processes of high-grade metal deposition in low-sulfidation epithermal deposits. Models for the formation of high-grade mineralization have to explain why compositional variations occur in nearly adjacent microspherical bands, unless rapid changes in metal supply to hydrothermal systems forming low-sulfidation epithermal deposits are invoked (Saunders et al., 2008; Simmons et al., 2016).

Model for the formation of microspherical colloform bands

Fournier (1985) showed that quartz deposition in the epithermal environment occurs in well-established hydrothermal systems characterized by slow cooling of the ascending hydrothermal solutions if the initial temperatures of the solutions were between ~200° and 340°C. In contrast, rapid cooling allows supersaturated silica solutions to form, particularly when cooling is predominately a result of decompressional boiling. Based on this, it is hypothesized here that the deposition of the noncrystalline silica that originally formed the microspherical colloform banding in the deposits of the Omu camp can be related to processes of fluid immiscibility. The occurrence of fluid immiscibility has long been recognized as an important process controlling precious metal deposition in many low-sulfidation epithermal deposits (Kamilli and Ohmoto, 1977; Drummond and Ohmoto, 1985; Hedenquist et al., 2000; Simmons and Browne, 2000; Simmons et al., 2005; Moncada et al., 2012, 2017). However, the results of this study indicate that while boiling is an important process, it is the intensity of vapor production that is a key control.

Moncada et al. (2012) suggested that two end-member types of fluid immiscibility can be distinguished in epithermal systems that differ in the intensity of vapor production. During decompressional boiling, a small amount of hydrothermal liquid is converted to vapor as the ascending hydrothermal liquid intersects the liquid plus vapor coexistence boundary. The small amount of vapor produced this way is buoyant and rises through the fracture network. The remaining liquid continues to ascend, producing small amounts of vapor. During more violent boiling, referred to as flashing, vapor is generated due to vaporization of a large amount of hydrothermal liquid (Scott and Watanabe, 1998; Moncada et al., 2012). Flashing, which may be triggered by a seismic event or dike-induced faulting (Rowland and Simmons, 2012), is associated with a change in pressure along the structure that controls the upflow of the hydrothermal fluids. As more and more vapor is produced in the upper part of the structure, pressure in the structure drops from hydrostatic to vaporstatic, and the lower pressure regime migrates downward as liquid flashes to vapor at depth and within the surrounding wall rock (Henley and Hughes, 2000). Rapid vaporization during flashing could cause widespread hydrothermal brecciation, potentially explaining the observation that the highest-grade samples from the Omu camp are brecciated.

Flashing of the hydrothermal liquids will result in deposition of noncrystalline silica, as silica solubility in the vapor phase is significantly lower than in the liquid (Monecke et al., 2018). Amagai et al. (2019) conducted a series of autoclave experiments to study the mechanisms of silica deposition associated with the flashing of silica-saturated fluids under hydrothermal conditions. During the experiments, noncrystal-

line silica microspheres were indeed formed at the outlet of the autoclave where the pressure drop occurred. Quartz was not formed in any of the experimental runs.

Deposition of noncrystalline silica during flashing may be accompanied by the formation of the ore minerals containing precious metals. During vaporization, H_2S strongly partitions into the vapor phase and the amount of H_2S in solution in the coexisting liquid will be significantly reduced. The resulting destabilization of gold bisulfide complexes results in gold precipitation (Brown, 1986; Sanchez-Alfaro et al., 2016). This process of metal deposition is observed in modern geothermal systems where a sharp decrease in pressure causing flashing occurs at the orifice plate within the head of production wells (Skinner et al., 1967; Brown, 1986; Karabelas et al., 1989; Akaku, 1990; Clark and Williams-Jones, 1990; Christanis and Seymour, 1995; Christenson and Hayba, 1995; Reyes et al., 2002; Hardardóttir et al., 2010). Sulfide formation may be accompanied by the deposition of noncrystalline silica, with some sulfides and noncrystalline silica being deposited in the steam lines as a result of deposition from liquid droplets that are carried over due to incomplete separation of vapor and liquid (Reyes et al., 2002).

Flashing is a highly dynamic process, and the degree of vapor production will vary with depth along the host structure and over time because of the changes in the pressure regime (Henley and Hughes, 2000). In a simplistic model of flashing, vapor flow will predominate in the shallow subsurface, although the vapor may carry droplets of the liquid. With increasing depth, vapor-dominated flow will transition to a region of two-phase flow. At greater depth, flow is dominated by the liquid. Deposition of silica and metals likely occurs within the region of two-phase flow where the chemistry of the ascending fluid changes rapidly.

Modeling of the process of vapor loss during flashing by Christenson and Hayba (1995) showed that different ore minerals are deposited within the region of two-phase flow as a function of the degrees of vapor formation. For instance, modeling of the isothermal vapor loss at 230°C by Christenson and Hayba (1995) demonstrated that sphalerite and pyrite precipitation starts with the onset of vapor loss in hydrothermal liquids. Sphalerite is stable throughout the process of vaporization, whereas pyrite is replaced by chalcopyrite at ~3 wt % vapor loss. Chalcopyrite is replaced by bornite and then chalcocite at 47 and 70 wt % vapor loss, respectively. Galena saturates at 3 wt % vapor loss and continues to precipitate throughout the process of vaporization. In the model of Christenson and Hayba (1995), Au precipitation starts at ~6 wt % vapor loss and continues to 90 wt % vapor loss. Accordingly, the highest Au grade is formed during the early stage of vapor loss (~10 wt %), but extensive (20–40 wt %) vapor loss is required to precipitate large amounts of Au. Although Christenson and Hayba (1995) did not model the formation of Ag sulfoselenides, their study suggests that differences in metal content and metal association in adjacent microspherical colloform bands might be related to differences in the amount of vapor formation. Other factors that perhaps influence ore mineral deposition during flashing events include changes in the flow pattern within the host structure (cf. Taitel et al., 1980) or the flow rate of the liquid through the microspherical substrate of the colloform bands.

Implications for exploration

The detailed microscopic work of this study showed that ore minerals in samples from the Omu camp are hosted in microspherical colloform bands and colloform bands of mosaic quartz that are the recrystallized equivalent. Textural evidence suggests that the development of bonanza-type grades in some low-sulfidation epithermal veins can be linked to flashing of the hydrothermal fluids. In the samples investigated, ore minerals were not typically associated with quartz textures that are a result of gentle boiling (cf. Moncada et al., 2012). This is important in mineral exploration, as some textures related to boiling, in particular the occurrence of bladed calcite replaced by quartz, can be readily recognized in hand specimen. In contrast, identification of the microspherical nature of colloform bands requires high-magnification optical microscopy.

Chemical mapping of hand specimens from the Omu camp demonstrates that the grade distribution varies significantly at the hand specimen scale. Microspherical colloform bands contain variable ore mineral assemblages. Macroscopically recognizable dark-gray to black ginguro bands are characterized by the abundance of Ag sulfoselenides and may or may not contain electrum. In these samples, electrum is primarily hosted within light-gray to white gankin bands of microspherical quartz or mosaic quartz formed through recrystallization. Without μXRF mapping, the gankin bands are not easily recognizable in hand specimen and cannot be macroscopically distinguished from barren chalcedonic colloform bands and mosaic quartz formed through recrystallization of the chalcedony. The observation that ginguro bands are not the only type of band containing ore minerals has important implications for grade estimation during exploration and potentially for grade control during the mining of low-sulfidation epithermal deposits.

The findings of this study also suggest that the depth of ore zones below the water table may be more difficult to predict than suggested by existing models of boiling-related metal deposition in low-sulfidation epithermal deposits. Previous thermodynamic considerations suggest that >90% of gold in boiling liquids deposits over a temperature range of 260° to 180°C (Simmons and Browne, 2000), which corresponds to a depth of ~470 to 100 m below paleosurface at cold hydrostatic conditions in the pure H_2O system. However, orebodies formed by flashing may theoretically occur over a wider depth range, as the pressure conditions change along the host structure during the flashing event.

Deep flashing of a hydrothermal system could result in the formation of bonanza-type grades from precious metals-laden hydrothermal liquids that have not previously experienced significant precious metal deposition as a result of cooling or boiling. Deep flashing may be possible where large faults control fluid flow, allowing propagation of vaporstatic pressures to depth during flashing events. In contrast, shallow flashing would tap into a reservoir of relatively low temperature hydrothermal fluids that could have lost much of the gold and silver they were originally carrying at depth as a result of cooling, gentle boiling, or both. As a result, shallow flashing does not likely result in the formation of bonanza-type grades. However, elevated precious metal grades may still develop

at shallow depth. Following the model of Saunders (1990), gold colloids may be produced as a result of flashing at depth and mechanically transported upward. Deposition of colloidal gold along the vein walls may result in grade development in the shallow subsurface all the way to paleosurface where the temperatures of the hydrothermal liquids are normally too low for significant gold transport in solution.

Conclusions

Low-sulfidation epithermal quartz veins of the Omu camp of Hokkaido exhibit a wide range of macroscopic and microscopic quartz textures. Crustiform and brecciated veins carry bonanza-grade precious metal grades with ore minerals occurring in distinct bands composed of colloform quartz. Petrographic investigations revealed the presence of relic microspheres within the colloform quartz bands that were originally composed of a noncrystalline, presumably gel-like silica precursor. Recrystallization of the microspherical colloform bands can result in the formation of colloform bands composed of mosaic quartz. The microspherical colloform bands are the principal host to ore minerals. Delicate intergrowth relationships suggest that electrum and the Ag sulfoselenides grew within the microspherical silica forming the colloform bands immediately after the silica deposition. The noncrystalline silica precursor and the ore minerals are interpreted to have formed during or shortly after short-lived episodes of flashing of the hydrothermal liquids. In contrast to the colloform quartz bands exhibiting relic microsphere textures and mosaic quartz formed through recrystallization, colloform bands composed of fibrous chalcedony and mosaic quartz that formed through recrystallization of the chalcedony are barren, recording periods during which flashing did not occur.

The finding of this study that fluid flashing can be responsible for the formation of bonanza-grade low-sulfidation epithermal veins has significant implications. Previous deposit models for low-sulfidation epithermal deposits emphasize the role of boiling as a mechanism of gold precipitation, implying that the location of ore zones can be predicted based on the depth of the onset of boiling, which can be recognized from fluid inclusion evidence or gangue mineral textures. However, if flashing is instead the principal process responsible for the formation of bonanza-grade precious metal enrichment, ore zones could theoretically occur over variable and potentially greater depths. The depth to which flashing occurs will depend primarily on the nature of the brittle structures controlling fluid flow and the hydraulic framework.

Acknowledgments

The authors thank the staff of Mitsui Mineral Development Engineering Co. and Irving Resources Inc. for logistical support in the field. In particular, we acknowledge Haruo Harada for assistance provided during the field work. We are indebted to Hidetoshi Takaoka and Akiko Levinson for advice and guidance throughout the course of this study. Thick section preparation was conducted by Jae Erickson and Sebastian Dettmar. We thank David Adams for performing the electron microprobe analyses. We are grateful to S. Simmons, an anonymous reviewer, and Associate Editor David John for their insightful reviews and comments, which helped improve an earlier version of this manuscript. This study was financially supported by Irving Resources Inc.

REFERENCES

Adams, S.F., 1920, A microscopic study of vein quartz: Economic Geology, v. 15, p. 623–664.

Akaku, K., 1990, Geochemical study on mineral precipitation from geothermal waters at the Fushime field, Kyushu, Japan: Geothermics, v. 19, p. 455–467.

Amagai, T., Okamoto, A., Niibe, T., Hirano, N., Motomiya, K., and Tsuchiya, N., 2019, Silica nanoparticles produced by explosive flash vaporization during earthquakes: Scientific Reports, v. 9, article 9738, doi: 10.1038/s41598-019-46320-7.

Aseto, C.O., 2012, Geology, geochemistry and geochronology of the mid-Miocene, low-sulfidation epithermal gold-silver ores on War Eagle Mountain, Silver City district, Idaho: Unpublished M.Sc. thesis, Auburn, Alabama, Auburn University, 170 p.

Barrett, C., Marsh, D., Bateman, S., Harada, H., and Inoue, T., 2018, Independent technical report on the Omu property, Hokkaido, Japan: Report prepared by SRK Exploration Services Ltd. and Mitsui Mineral Development Engineering Company Ltd., 63 p., https://www.irvresources.com/assets/docs/projects/ES7783_Irving%20Japan%20NI%2043-101_v2-0-final.pdf.

Bettermann, P., and Liebau, F., 1975, The transformation of amorphous silica to crystalline silica under hydrothermal conditions: Contributions to Mineralogy and Petrology, v. 53, p. 25–36.

Bobis, R.E., 1994, A review of the description, classification and origin of quartz textures in low sulphidation epithermal veins: Journal of the Geological Society of the Philippines, v. 49, p. 15–39.

Brown, K.L., 1986, Gold deposition from geothermal discharges in New Zealand: Economic Geology, v. 81, p. 979–983.

——2011, Thermodynamics and kinetics of silica scaling [ext. abs.]: International Workshop on Mineral Scaling, Manila, Philippines, 2011, Proceedings, 8 p.

Campbell, K.A., Sannazzaro, K., Rodgers, K.A., Herdianita, N.R., and Browne, P.R.L., 2001, Sedimentary facies and mineralogy of the late Pleistocene Umukuri silica sinter, Taupo volcanic zone, New Zealand: Journal of Sedimentary Research, v. 71, p. 727–746.

Campbell, K.A., Rodgers, K.A., Brotheridge, J.M.A., and Browne, P.R.L., 2002, An unusual modern silica-carbonate sinter from Pavlova spring, Ngatamariki, New Zealand: Sedimentology, v. 49, p. 835–854.

Camprubí, A., and Albinson, T., 2007, Epithermal deposits in México—update of current knowledge, and an empirical reclassification: Geological Society of America, Special Paper 422, p. 377–415.

Christanis, K., and Seymour, K.S., 1995, A study of scale deposition: An analogue of meso- to epithermal ore formation in the volcano of Milos, Aegean arc, Greece: Geothermics, v. 24, p. 541–552.

Christenson, B.W., and Hayba, D.O., 1995, Hydrothermal eruptions in ore forming reservoirs: Analogues and models [ext. abs.]: Exploring the Rim, PACRIM Congress, Auckland, New Zealand, 1995, Proceedings, p. 119–124.

Clark, J.R., and Williams-Jones, A.E., 1990, Analogues of epithermal gold-silver deposition in geothermal well scales: Nature, v. 346, p. 644–645.

Dong, G., Morrison, G., and Jaireth, S., 1995, Quartz textures in epithermal veins, Queensland—classification, origin, and implication: Economic Geology, v. 90, p. 1841–1856.

Drummond, S.E., and Ohmoto, H., 1985, Chemical evolution and mineral deposition in boiling hydrothermal systems: Economic Geology, v. 80, p. 126–147.

Ernst, W.G., and Calvert, S.E., 1969, An experimental study of the recrystallization of porcelanite and its bearing on the origin of some bedded cherts: American Journal of Science, v. 267, p. 114–133.

Etoh, J., Izawa, E., Watanabe, K., Taguchi, S., and Sekine, R., 2002, Bladed quartz and its relationship to gold mineralization in the Hishikari low-sulfidation epithermal gold deposit, Japan: Economic Geology, v. 97, p. 1841–1851.

Faure, K., Matsuhisa, Y., Metsugi, H., Mizota, C., and Hayashi, S., 2002, The Hishikari Au-Ag epithermal deposit, Japan: Oxygen and hydrogen isotope evidence in determining the source of paleohydrothermal fluids: Economic Geology, v. 97, p. 481–498.

Fernandez-Turiel, J.L., Garcia-Valles, M., Gimeno-Torrente, D., Saavedra-Alonso, J., and Martinez-Manent, S., 2005, The hot spring and geyser sinters of El Tatio, northern Chile: Sedimentary Geology, v. 180, p. 125–147.

Fournier, R.O., 1985, The behavior of silica in hydrothermal solutions: Reviews in Economic Geology, v. 2, p. 45–61.
Gallup, D.L., 1997, Aluminum silicate scale formation and inhibition: Scale characterization and laboratory experiments: Geothermics, v. 26, p. 483–499.
Gudmundsson, J.S., and Bott, T.R., 1979, Deposition of silica from geothermal waters on heat transfer surfaces: Desalination, v. 28, p. 125–145.
Guidry, S.A., and Chafetz, H.S., 2003, Anatomy of siliceous hot springs: Examples from Yellowstone National Park, Wyoming, USA: Sedimentary Geology, v. 157, p. 71–106.
Hardardóttir, V., Hannington, M., Hedenquist, J., Kjarsgaard, I., and Hoal, K., 2010, Cu-rich scales in the Reykjanes geothermal system, Iceland: Economic Geology, v. 105, p. 1143–1155.
Hedenquist, J.W., Arribas, A., and Gonzalez-Urien, E., 2000, Exploration for epithermal gold deposits: Reviews in Economic Geology, v. 13, p. 245–277.
Henley, R.W., and Hughes, G.O., 2000, Underground fumaroles: "Excess heat" effects in vein formation: Economic Geology, v. 95, p. 453–466.
Herdianita, N.R., Browne, P.R.L., Rodgers, K.A., and Campbell, K.A., 2000, Mineralogical and textural changes accompanying ageing of silica sinter: Mineralium Deposita, v. 35, p. 48–62.
Izawa, E., Urashima, Y., Ibaraki, K., Suzuki, R., Yokoyama, T., Kawasaki, K., Koga, A., and Taguchi, S., 1990, The Hishikari gold deposit: High-grade epithermal veins in Quaternary volcanics of southern Kyushu, Japan: Journal of Geochemical Exploration, v. 36, p. 1–56.
Jackson, E.D., Shaw, H.R., and Bargar, K.E., 1975, Calculated geochronology and stress field orientations along the Hawaiian Chain: Earth and Planetary Science Letters, v. 26, p. 145–155.
Jamero, J., Zarrouk, S.J., and Mrozek, E., 2018, Mineral scaling in two-phase geothermal pipelines: Two case studies: Geothermics, v. 72, p. 1–14.
Jones, B., Renaut, R.W., and Rosen, M.R., 1997, Biogenicity of silica precipitation around geysers and hot-spring vents, North Island, New Zealand: Journal of Sedimentary Research, v. 67, p. 88–104.
Kamilli, R.J., and Ohmoto, H., 1977, Paragenesis, zoning, fluid inclusions, and isotopic studies of the Finlandia vein, Colqui district, central Peru: Economic Geology, v. 72, p. 950–982.
Karabelas, A.J., Andritsos, N., Mouza, A., Mitrakas, M., Vrouz, F., and Christanis, K., 1989, Characteristics of scales from the Milos geothermal plant: Geothermics, v. 18, p. 169–174.
Kimura, G., and Tamaki, K., 1986, Collision, rotation, and back-arc spreading in the region of the Okhotsk and Japan Seas: Tectonics, v. 5, p. 389–401.
Koshimizu, S., and Kim, C.W., 1987, Fission-track dating of the Cenozoic formations in central-eastern Hokkaido, Japan (part IV)—terrestrial pyroclastics: Journal of the Geological Society of Japan, v. 93, p. 217–227.
Leavitt, E.D., Spell, T.L., Goldstrand, P.M., and Arehart, G.B., 2004, Geochronology of the Midas low-sulfidation epithermal gold-silver deposit, Elko County, Nevada: Economic Geology, v. 99, p. 1665–1686.
Lovering, T.G., 1972, Jasperoid in the United States—its characteristics, origin, and economic significance: U.S. Geological Survey, Professional Paper 710, 164 p.
Lynne, B.Y., and Campbell, K.A., 2004, Morphologic and mineralogic transitions from opal-A to opal-CT in low-temperature siliceous sinter diagenesis, Taupo volcanic zone, New Zealand: Journal of Sedimentary Research, v. 74, p. 561–579.
Lynne, B.Y., Campbell, K.A., Moore, J.N., and Browne, P.R.L., 2005, Diagenesis of 1900-year-old siliceous sinter (opal-A to quartz) at Opal Mound, Roosevelt Hot Springs, Utah, U.S.A.: Sedimentary Geology, v. 179, p. 249–278.
Lynne, B.Y., Campbell, K.A., James, B.J., Browne, P.R.L., and Moore, J., 2007, Tracking crystallinity in siliceous hot-spring deposits: American Journal of Science, v. 307, p. 612–641.
Maeda, H., 1997, K-Ar age of mercury mineralization and related volcanic activity in Kitami metallogenic province, Hokkaido, Japan: Specimens from Asahino disseminated- and Tokoro vein-type mercury deposits: Resource Geology, v. 47, p. 11–20.
Marinova, I., Ganev, V., and Titorenkova, R., 2014, Colloidal origin of colloform-banded textures in the Paleogene low-sulfidation Khan Krum gold deposit, SE Bulgaria: Mineralium Deposita, v. 49, p. 49–74.
Matsuhisa, Y., and Aoki, M., 1994, Temperature and oxygen isotope variations during formation of the Hishikari epithermal gold-silver veins, southern Kyushu, Japan: Economic Geology, v. 89, p. 1608–1613.
Meier, D.B., Gunnlaugsson, E., Gunnarsson, I., Jamtveit, B., Peacock, C.L., and Benning, L.G., 2014, Microstructural and chemical variation in silica-rich precipitates at the Hellisheiði geothermal power plant: Mineralogical Magazine, v. 78, p. 1381–1389.
Miehe, G., Graetsch, H., and Flörke, O.W., 1984, Crystal structure and growth fabric of length-fast chalcedony: Physics and Chemistry of Minerals, v. 10, p. 197–199.
Milliard, J.B., Marma, J.C., Kassos, G., Hobbs, E., Borchardt, J.S., and Rehak, K.R., 2015, Geology of the Fire Creek exploration project—low-sulfidation epithermal bonanza gold-silver deposit, Lander County, Nevada, USA [ext. abs.]: Geological Society of Nevada 2015 Symposium, Reno, Nevada, USA, 2015, Proceedings, p. 1339–1364.
Moncada, D., Mutchler, S., Nieto, A., Reynolds, T.J., Rimstidt, J.D., and Bodnar, R.J., 2012, Mineral textures and fluid inclusion petrography of the epithermal Ag-Au deposits at Guanajuato, Mexico: Application to exploration: Journal of Geochemical Exploration, v. 114, p. 20–35.
Moncada, D., Baker, D., and Bodnar, R.J., 2017, Mineralogical, petrographic and fluid inclusion evidence for the link between boiling and epithermal Ag-Au mineralization in the La Luz area, Guanajuato mining district, México: Ore Geology Reviews, v. 89, p. 143–170.
Monecke, T., Monecke, J., Reynolds, T.J., Tsuruoka, S., Bennett, M.M., Skewes, W.B., and Palin, R., 2018, Quartz solubility in the H_2O-NaCl system: A framework for understanding vein formation in porphyry copper deposits: Economic Geology, v. 113, p. 1007–1046.
Mukaiyama, H., 1950, On some gold-silver ores from the Sado mine, Sado Island, Niigata Prefecture, Japan: Journal of the Geological Society of Japan, v. 56, p. 181–187.
Nash, J.T., Utterback, W.C., and Saunders, J.A., 1989, Geology and geochemistry of the Sleeper gold-silver deposit, Humboldt County, Nevada—an interim report: U.S. Geological Survey, Open-File Report 89-476, 39 p.
Oehler, J.H., 1976, Hydrothermal crystallization of silica gel: Geological Society of America Bulletin, v. 87, p. 1143–1152.
Okada, H., 1982, Geological evolution of Hokkaido, Japan: An example of collision orogenesis: Proceedings of the Geologists' Association, v. 93, p. 201–212.
Raymond, J., Williams-Jones, A.E., and Clark, J.R., 2005, Mineralization associated with scale and altered rock and pipe fragments from the Berlín geothermal field, El Salvador; implications for metal transport in natural systems: Journal of Volcanology and Geothermal Research, v. 145, p. 81–96.
Reyes, A.G., Trompetter, W.J., Britten, K., and Searle, J., 2002, Mineral deposits in the Rotokawa geothermal pipelines, New Zealand: Journal of Volcanology and Geothermal Research, v. 119, p. 215–239.
Rodgers, K.A., Browne, P.R.L., Buddle, T.F., Cook, K.L., Greatrex, R.A., Hampton, W.A., Herdianita, N.R., Holland, G.R., Lynne, B.Y., Martin, R., Newton, Z., Pastars, D., Sannazarro, K.L., and Teece, C.I.A., 2004, Silica phases in sinters and residues from geothermal fields of New Zealand: Earth-Science Reviews, v. 66, p. 1–61.
Rogers, A.F., 1917, A review of the amorphous minerals: Journal of Geology, v. 25, p. 515–541.
Rothbaum, H.P., Anderton, B.H., Harrison, R.F., Rohde, A.G., and Slatter, A., 1979, Effect of silica polymerisation and pH on geothermal scaling: Geothermics, v. 8, p. 1–20.
Rowland, J.V., and Simmons, S.F., 2012, Hydrologic, magmatic, and tectonic controls on hydrothermal flow, Taupo volcanic zone, New Zealand: Implications for the formation of epithermal vein deposits: Economic Geology, v. 107, p. 427–457.
Sanchez-Alfaro, P., Reich, M., Driesner, T., Cembrano, J., Arancibia, G., Pérez-Flores, P., Heinrich, C.A., Rowland, J., Tardani, D., Lange, D., and Campos, E., 2016, The optimal windows for seismically-enhanced gold precipitation in the epithermal environment: Ore Geology Reviews, v. 79, p. 463–473.
Sander, M.V., and Black, J.E., 1988, Crystallization and recrystallization of growth-zoned vein quartz crystals from epithermal systems—implications for fluid inclusion studies: Economic Geology, v. 83, p. 1052–1060.
Sanematsu, K., Watanabe, K., Duncan, R.A., and Izawa, E., 2006, The history of vein formation determined by $^{40}Ar/^{39}Ar$ dating of adularia in the Hosen-1 vein at the Hishikari epithermal gold deposit, Japan: Economic Geology, v. 101, p. 685–698.
Saunders, J.A., 1990, Colloidal transport of gold and silica in epithermal precious-metal systems: Evidence from the Sleeper deposits, Nevada: Geology, v. 18, p. 757–760.
——1994, Silica and gold textures in bonanza ores of the Sleeper deposit, Humboldt County, Nevada: Evidence for colloids and implications for epithermal ore-forming processes: Economic Geology, v. 89, p. 628–638.
——2012, Textural evidence of episodic introduction of metallic nanoparticles into bonanza epithermal ores: Minerals, v. 2, p. 228–243.

Saunders, J.A., and Schoenly, P.A., 1995, Boiling, colloid nucleation and aggregation, and the genesis of bonanza Au-Ag ores of the Sleeper deposit, Nevada: Mineralium Deposita, v. 30, p. 199–210.
Saunders, J.A., Unger, D.L., Kamenov, G.D., Fayek, M., Hames, W.E., and Utterback, W.C., 2008, Genesis of Middle Miocene Yellowstone hotspot-related bonanza epithermal Au-Ag deposits, Northern Great Basin, USA: Mineralium Deposita, v. 43, p. 715–734.
Saunders, J.A., Beasley, L., Vikre, P., and Unger, D.L., 2011, Colloidal and physical transport textures exhibited by electrum and naumannite in bonanza epithermal veins from western USA, and their significance [ext. abs.]: Geological Society of Nevada 2010 Symposium, Reno-Sparks, Nevada, USA, 2010, Proceedings, p. 825–832.
Scott, A.M., and Watanabe, Y., 1998, "Extreme boiling" model for variable salinity of the Hokko low-sulfidation epithermal Au prospect, southwestern Hokkaido, Japan: Mineralium Deposita, v. 33, p. 568–578.
Sherlock, R.L., and Lehrman, N.J., 1995, Occurrences of dendritic gold at the McLaughlin mine hot-spring gold deposit: Mineralium Deposita, v. 30, p. 323–327.
Shimada, N., Nakamura, T., Morinaga, Y., and Shikama, Y., 2005, Invisible gold from the Hishikari epithermal gold deposit, Japan: Implication for gold distribution and deposition: Resource Geology, v. 55, p. 91–100.
Shimizu, T., 2014, Reinterpretation of quartz textures in terms of hydrothermal fluid evolution at the Koryu Au-Ag deposit, Japan: Economic Geology, v. 109, p. 2051–2065.
Shimizu, T., Matsueda, H., Ishiyama, D., and Matsubaya, O., 1998, Genesis of epithermal Au-Ag mineralization of the Koryu mine, Hokkaido, Japan: Economic Geology, v. 93, p. 303–325.
Simmons, S.F., and Browne, P.R.L., 2000, Hydrothermal minerals and precious metals in the Broadlands-Ohaaki geothermal system: Implications for understanding low-sulfidation epithermal environments: Economic Geology, v. 95, p. 971–999.
Simmons, S.F., White, N.C., and John, D.A., 2005, Geological characteristics of epithermal precious and base metal deposits: Economic Geology 100th Anniversary Volume, p. 485–522.
Simmons, S.F., Brown, K.L., and Tutolo, B.M., 2016, Hydrothermal transport of Ag, Au, Cu, Pb, Te, Zn, and other metals and metalloids in New Zealand geothermal systems: Spatial patterns, fluid-mineral equilibria, and implications for epithermal mineralization: Economic Geology, v. 111, p. 589–618.
Skinner, B.J., White, D.E., Rose, H.J., and Mays, R.E., 1967, Sulfides associated with the Salton Sea geothermal brine: Economic Geology, v. 62, p. 316–330.
Suzuki, M., Kōnoya, M., and Fujiwara, T., 1966, Explanatory text of the geological map of Japan (scale 1:50,000): Omu (Abashiri-6): Sapporo, Hokkaido, Japan, Geological Survey of Hokkaido, 25 p.
Taitel, Y., Bornea, D., and Dukler, A.E., 1980, Modelling flow pattern transitions for steady upward gas-liquid flow in vertical tubes: AIChE Journal, v. 26, p. 345–354.
Takanashi, K., Kakihara, Y., Ishimoto, H., and Shuto, K., 2012, Melting of crustal rocks as a possible origin for Middle Miocene to Quaternary rhyolites of northeast Hokkaido, Japan: Constraints from Sr and Nd isotopes and major- and trace-element chemistry: Journal of Volcanology and Geothermal Research, v. 221–222, p. 52–70.
Takeuchi, K., and Shikazono, N., 1984, Mineralization of the Arakawa No. 4 vein of the Kushikino mine, Kagoshima Prefecture, Japan: Mining Geology, v. 34, p. 187–195.
Taksavasu, T., Monecke, T., and Reynolds, T.J., 2018, Textural characteristics of noncrystalline silica in sinters and quartz veins: Implications for the formation of bonanza veins in low-sulfidation epithermal deposits: Minerals, v. 8, article 331, doi: 10.3390/min8080331.
Tharalson, E.R., Monecke, T., Reynolds, T.J., Zeeck, L., Pfaff, K., and Kelly, N.M., 2019, The distribution of precious metals in high-grade banded quartz veins from low-sulfidation epithermal deposits: Constraints from μXRF mapping: Minerals, v. 9, article 740, doi: 10.3390/min9120740.
Unger, D.L., 2008, Geochronology and geochemistry of mid-Miocene bonanza low-sulfidation epithermal ores of the northern Great Basin, USA: Unpublished M.Sc. thesis, Auburn, Alabama, Auburn University, 133 p.
van den Heuvel, D.B., Gunnlaugsson, E., Gunnarsson, I., Stawski, T.M., Peacock, C.L., and Benning, L.G., 2018, Understanding amorphous silica scaling under well-constrained conditions inside geothermal pipelines: Geothermics, v. 76, p. 231–241.
Watanabe, Y., 1995, A tectonic model for epithermal Au mineralization in NE Hokkaido, Japan: Resource Geology Special Issue, v. 18, p. 257–269.
——1996, Genesis of vein-hosting fractures in the Kitami region, Hokkaido, Japan: Resource Geology, v. 46, p. 151–166.
Watanabe, Y., and Iwata, K., 1987, The Hidaka Supergroup in the Tomuraushi region, Hidaka belt, Hokkaido, Japan: Earth Science (Chikyu Kagaku), v. 41, p. 35–47.
Watanabe, Y., and Yamaguchi, S., 1988, K-Ar ages of Miocene volcanic rocks and the tectonics in the Nayoro-Asahikawa region, northern Hokkaido: Earth Science (Chikyu Kagaku), v. 42, p. 91–99.
Watanabe, Y., Uchiumi, S., and Uto, K., 1991, K-Ar ages of Neogene basalts in Kitami green tuff region, northeast Hokkaido: Journal of the Geological Society of Japan, v. 97, p. 61–64.
Yokoyama, T., Sato, Y., Maeda, Y., Tarutani, T., and Itoi, R., 1993, Siliceous deposits formed from geothermal water. I. The major constituents and the existing states of iron and aluminum: Geochemical Journal, v. 27, p. 375–384.
Zarrouk, S.J., Woodhurst, B.C., and Morris, C., 2014, Silica scaling in geothermal heat exchangers and its impact on pressure drop and performance: Wairakei binary plant, New Zealand: Geothermics, v. 51, p. 445–459.

Lauren Zeeck currently is a Ph.D. student in geology at the Center for Mineral Resources Science at Colorado School of Mines, Golden, Colorado. She obtained an undergraduate degree at the University of Colorado Boulder in 2013 and subsequently worked as a contract geologist in Japan and the United States. In 2018, she graduated with an M.S. degree in geology from Colorado School of Mines, with her thesis focusing on the geology of the low-sulfidation epithermal deposits of the Omu camp in Hokkaido.